Alzheimer's Research & Therapy

RESEARCH

Open Access

# Increased excitability of dentate gyrus mossy cells occurs early in life in the Tg2576 model of Alzheimer's disease

David Alcantara-Gonzalez[1,2*], Meghan Kennedy[1], Chiara Criscuolo[1,2], Justin Botterill[4] and Helen E. Scharfman[1,2,3*]

## Abstract

**Background** Hyperexcitability in Alzheimer's disease (AD) is proposed to emerge early and contribute to disease progression. The dentate gyrus (DG) and its primary cell type, granule cells (GCs) are implicated in hyperexcitability in AD. Hence, we hypothesized that mossy cells (MCs), important regulators of GC excitability, contribute to early hyperexcitability in AD. Indeed, MCs and GCs are linked to hyperexcitability in epilepsy.

**Methods** Using the Tg2576 model of AD and WT mice (~ 1 month-old), we compared MCs and GCs electrophysiologically and morphologically, assessed the activity marker c-Fos, Aβ expression and a hippocampal- and MC-dependent memory task that is impaired at 3–4 months of age in Tg2576 mice.

**Results** Tg2576 MCs had increased spontaneous excitatory events (sEPSP/Cs) and decreased spontaneous inhibitory currents (sIPSCs), increasing the excitation/inhibition ratio. Additionally, Tg2576 MC intrinsic excitability was enhanced. Consistent with in vitro results, Tg2576 MCs showed enhanced c-Fos protein expression. Tg2576 MCs had increased intracellular Aβ expression, suggesting a reason for increased excitability. GCs showed increased excitatory and inhibitory input without changes in intrinsic properties, consistent with effects of increased MC activity. In support, increased GC activity was normalized by an antagonist of MC input to GCs. Also in support, Tg2576 MC axons showed sprouting to the area of GC dendrites. These effects occurred before an impairment in the memory task, suggesting they are extremely early alterations.

**Conclusions** Alterations in Tg2576 MCs and GCs early in life suggest an early role for MCs in increased GC excitability. MCs may be a novel target to intervene in AD pathophysiology at early stages.

**Keywords** Hyperexcitability, Synaptic properties, Intrinsic properties, Granule cells, hAPP, Intracellular Aβ, Novel object recognition, Spatial memory, Hippocampal slices, c-Fos expression

*Correspondence:
David Alcantara-Gonzalez
David.alcantarag@nki.rfmh.org
Helen E. Scharfman
hscharfman@nki.rfmh.org
[1]Center for Dementia Research, The Nathan Kline Institute for Psychiatric Research, 140 Old Orangeburg Rd. Bldg. 39, Orangeburg, NY 10962, USA
[2]Department of Child & Adolescent Psychiatry, Neuroscience & Physiology, and Psychiatry, New York University Langone Health, New York City, NY 10016, USA
[3]Neuroscience Institute, New York University Langone Health, New York City, NY 10016, USA
[4]College of Medicine, University of Saskatchewan, Saskatoon, SK, Canada

© The Author(s) 2025. **Open Access** This article is licensed under a Creative Commons Attribution-NonCommercial-NoDerivatives 4.0 International License, which permits any non-commercial use, sharing, distribution and reproduction in any medium or format, as long as you give appropriate credit to the original author(s) and the source, provide a link to the Creative Commons licence, and indicate if you modified the licensed material. You do not have permission under this licence to share adapted material derived from this article or parts of it. The images or other third party material in this article are included in the article's Creative Commons licence, unless indicated otherwise in a credit line to the material. If material is not included in the article's Creative Commons licence and your intended use is not permitted by statutory regulation or exceeds the permitted use, you will need to obtain permission directly from the copyright holder. To view a copy of this licence, visit http://creativecommons.org/licenses/by-nc-nd/4.0/.

## Background

Alzheimer's disease (AD) is a neurodegenerative and progressive disorder characterized by memory impairment, and by the presence of amyloid β (Aβ) plaques and neurofibrillary tangles [1–4]. Despite extensive efforts, medications to treat AD are still needed. Several clinical studies suggest that treatment is most effective when started at early stages of AD. Therefore, it is relevant to understand the earliest contributing factors to AD.

Clinical findings suggest hyperexcitability is a characteristic of AD, often occurring at early stages, such as mild cognitive impairment (MCI) [5–11]. In patients, neuronal hyperexcitability is reflected by enhanced brain activity on fMRI when performing a memory-encoding task [12, 13], and by epileptiform activity and intermittent seizures [5–10, 14, 15]. Hyperexcitability is also present in mouse models of AD, which show intermittent seizures, interictal spikes, and high frequency oscillations, which are hallmarks of epilepsy [5, 16–25]. In addition, there is a reduction in the threshold for generating seizures in rodent models that simulate AD [26–28]. Interestingly, it was shown that reducing neuronal excitability can rescue the cognitive impairments in several mouse models [16, 29–34], and it also can reduce Aβ load, preventing the spread of Aβ pathology in the brain [21]. However, the underlying mechanisms of hyperexcitability and their importance to AD pathophysiology are not fully understood [7, 9, 14, 15].

An important area for studying hyperexcitability is the hippocampus because it is an early site for AD pathology [13] and is involved in seizure generation in temporal lobe epilepsy (TLE) [23, 25, 35, 36]. In particular, the hippocampal dentate gyrus (DG) has been suggested to be important in AD [37]. The DG is normally characterized by low excitability [38, 39], a product of the intrinsic properties of the main DG cell type, the granule cells (GCs) [38, 40, 41] and strong inhibition of GCs mediated by GABAergic interneurons [42–44]. As a result, the DG has been considered as a gate that regulates seizures in TLE [45, 46]. When DG excitability is increased as it is in AD, the normal role of the DG in spatial memory and other cognitive functions (such as pattern separation and novelty detection) are impaired [38, 47–50].

Tg2576 mice are an AD model that overexpresses a specific mutation in the amyloid precursor protein (APP; APPSwe) and are characterized by a relatively slow progression of AD pathology [51–54], so one can study early stages. We previously showed that interictal spikes occur in vivo as early as 1 month of age, long before memory deficits and Aβ plaques [23]. When GCs were recorded in hippocampal slices in ~3 month-old Tg2576 mice, they showed increased excitatory synaptic input, as well as changes in some intrinsic properties, which might be compensatory [55]. Therefore, we asked if the increased synaptic input to GCs might occur at earlier ages without altered intrinsic properties because time had not allowed for compensatory changes. We also asked what might be causing changes in synaptic input. We hypothesized increased excitation was caused by mossy cells (MCs), one of the main excitatory inputs to GCs..

MCs are glutamatergic neurons in the DG hilus that represent the primary excitatory input to the GC proximal dendrites and constitute about 35% of all DG neurons [56–62]. MCs directly innervate GCs [63–65], but also DG interneurons [63], so the net effect of MCs on GCs has never been clear. An initial hypothesis was that the net effect of MCs on GCs is inhibitory because loss of MCs in an experimental model of epilepsy led to GC hyperexcitability [66, 67]. That idea was supported by later studies that killed mossy cells selectively and found GC hyperexcitability followed [68]. However, the initial work in experimental epilepsy killed mossy cells as well as GABAergic neurons, making it unclear if MC loss led to GC hyperexcitability, or it was due to loss of GABAergic neurons. The later work by Jinde and colleagues that selectively killed MCs only found transient hyperexcitability in GCs for reasons that are unclear. More studies supported the idea that the net effect of MCs on GCs is inhibitory [69] but under some conditions the net effect of MCs on GCs is excitatory [70]. One reason may be that the pharmacology and synaptic plasticity of the MC→GC synapse differs from the MC→GABAergic neuron synapse [71, 72]. Although MCs have been studied in several diseases [49, 69, 70, 73], their contribution to AD has been rarely studied.

To study MCs and GCs at high resolution, we conducted whole cell recordings in hippocampal slices at 1 month of age and characterized spontaneous excitatory and inhibitory postsynaptic events (i.e., sEPSPs, sEPSCs and sIPSCs) and intrinsic properties (e.g., resting membrane potential, input resistance, etc.). Our results suggest that MCs have increased excitability at just 1 month of age. This was reflected in their sPSP/Cs, and also in an increased mean firing frequency in response to current injected intracellularly. MCs showed increased c-Fos protein in Tg2576 mice, consistent with in vitro results. Tg2576 MCs also showed high cytoplasmic Aβ protein, suggesting a possible reason for their alterations. GCs showed altered synaptic events, some of which were mitigated by inhibiting the MC synapses with GCs. Consistent with those results, MC axons of Tg2576 mice showed sprouting in the location of GC dendrites. GCs did not exhibit altered intrinsic properties, suggesting their earliest changes are synaptic. Finally, a hippocampal-dependent behavioral task, novel object recognition, was not impaired at 1 month of age despite being impaired later in life, suggesting changes in MCs occur before cognitive deficits.

## Methods

### Animals

All experimental procedures were carried out in accordance with the National Institutes of Health (NIH) guidelines and approved by the Institutional Animal Care and Use Committee (IACUC) at The Nathan Kline Institute. For Tg2576 mice expressing human $APP_{695}$ with the Swedish (Lys670Arg, Met671Leu) mutations driven by the hamster prion protein promoter [51], male and female mice were obtained from crossing male heterozygous Tg2576 and female non-transgenic mice (C57BL6/SJL F1 hybrid, stock No. 100012, Jackson Labs). For Tg2576 and WT mice that expressed Cre-recombinase in cells with the dopaminergic D2 receptor (*Drd2*-cre), $Tg2576^{+/-}$ males were crossed with *Drd2*-$cre^{+/-}$ females (age range: 2–5 months). Breeders were fed a standard rodent chow (Purina 5008, W.F. Fisher). Offspring were housed with same-sex siblings, provided 2″× 2″ nestlets (W.F. Fisher), and fed rodent food after weaning (Purina 5001, W.F. Fisher). Food and water were available *ad libitum*, with a 12 h light-dark cycle. Genotypes for the $APP_{695}$ gene and Cre gene were determined using standard protocols (New York University Mouse Genotyping Core) in Tg2576 mice and Tg2576 x *Drd2*-Cre mice.

### Slice electrophysiology

#### *Slice Preparation*

Mice were deeply anesthetized by isoflurane (Pivetal, Aspen Veterinary Resources) inhalation, followed by an intraperitoneal (i.p.) injection of urethane (2.5 g/kg; Sigma-Aldrich) dissolved in 0.9% NaCl. Subsequently, mice were intracardially perfused with a cold (4°C) sucrose-based artificial cerebrospinal fluid (sucrose ACSF) containing (in mM): 90 sucrose, 2.5 KCl, 1.25 $NaH_2PO_4$, 4.5 $MgSO_4$, 25.0 $NaHCO_3$, 10.0 D-glucose, 80.0 NaCl, and 0.5 $CaCl_2$, pH 7.4; constantly aerated with carbogen (95% $O_2$, 5% $CO_2$, All-Weld Products). The brain was quickly removed and dissected in sucrose ACSF at 4°C. Horizontal hippocampal slices (350 µm thick) were obtained using the same cold sucrose ACSF with a vibratome (VT1200S, Leica). Slices were immediately placed in a custom-made holding chamber containing sucrose ACSF at 30°C for 20 min and aerated with carbogen (95% $O_2$, 5% $CO_2$). Then, the slices were transferred to normal recording ACSF (NaCl ACSF; containing NaCl instead of sucrose, in mM: 130 NaCl, 2.5 KCl, 1.25 $NaH_2PO_4$, 1 $MgSO_4$, 25.0 $NaHCO_3$, 10.0 D-glucose, and 2.4 $CaCl_2$; pH 7.4) at room temperature for at least 60 min before recording.

#### *Whole-cell patch clamp recordings*

**Recording acquisition** Slices were transferred to a recording chamber (RC-27LD, Warner) and perfused with NaCl ACSF at 6 mL/min with a peristaltic pump (Masterflex C/L, Cole-Parmer) and maintained at 32°C with a temperature controller (TC-324B, Warner) and in-line heater (SH-27B, Warner). For whole cell patch-clamp recordings, borosilicate glass capillaries (1.5 mm outer diameter and 0.86 mm inner diameter, Sutter Instruments) were pulled horizontally (P-97, Sutter) with a resistance of 4–9 MΩ. Current-clamp recordings were performed with a potassium ($K^+$)-gluconate based intracellular solution containing (in mM; all reagents from Sigma-Aldrich): 130.0 $K^+$-gluconate, 4.0 KCl, 2.0 NaCl, 10.0 HEPES, 0.2 EGTA, 4.0 Mg-ATP, 0.3 $Na_2$-GTP, 14.0 Tris-phosphocreatine, and 0.5% biocytin (pH 7.3 and 295 ± 5 mOsm). Voltage-clamp recordings were done using cesium ($Cs^+$)-methanesulfonate intracellular solution of the following composition (in mM): 125 $Cs^+$-methanesulfonate, 4 NaCl, 10 HEPES, 1 EGTA, 4 Mg-ATP, 0.3 Tris-GTP, 10 diTris-phosphocreatine, 5 QX-314 chloride, and 0.5% biocytin (pH 7.3 and 300 ± 5 mOsm). Seal resistances were >1 GΩ before breaking into whole cell configuration. All data were digitized (Digidata 1440 A, Molecular Devices), amplified by a MultiClamp 700B amplifier (Molecular Devices), and low pass-filtered using a single-pole RC filter at 10 kHz. For every recording, before approaching a cell, the automatic Pipette Offset option in pClamp software was used to zero the potential (autozero) to correct for liquid junction potentials. No extra adjustments were performed. The mean adjustment was 48.70 ± 2.30 mV for the current clamp experiments ($K^+$-gluconate-based internal solution) and −74.20 ± 1.10 mV ($Cs^+$-methanesulphonate-based internal solution). All the ionic constituents of the internal solutions and ACSF were constant in any given experiment. For the evaluation of synaptic activity, spontaneous events were recorded continuously for 3–5 min. Cells were included if access resistance did not change more than 20%. Data acquisition used pClamp software (v11.2, Molecular Devices) and data analysis was performed using Clampfit software (v11.2, Molecular Devices), as described further below.

#### *Spontaneous synaptic potentials and synaptic currents*

Current-clamp recordings of spontaneous excitatory postsynaptic potentials (sEPSPs) were obtained from MCs and GCs using the $K^+$-gluconate intracellular solution. Spontaneous EPSPs were evaluated at resting membrane potential (RMP). Voltage-clamp recordings of spontaneous excitatory and inhibitory postsynaptic currents (sEPSCs and sIPSCs, respectively) were performed in a different set of neurons, using the $Cs^+$-methanesulfonate intracellular solution. Different holding potentials (HP) were used for isolating the different types of currents. To record sIPSCs, cells were voltage-clamped at a HP of +10 mV, and to evaluate AMPA- and

NMDA-sEPSCs, cells were voltage-clamped at a HP -70 mV and – 30 mV, respectively.

Detection of spontaneous events (sEPSPs, sEPSCs and sIPSCs) was performed off-line using MiniAnalysis 6.0 (Synaptosoft, Inc.) and the criteria described previously [55]. Briefly, sEPSPs, sEPSCs and sIPSCs were identified as events having a fast rise time, and were included if the maximum (peak) voltage (depolarizing, for EPSPs) or current (negative or positive, for EPSCs and IPSCs, respectively) was larger than 3 standard deviations (SD) from the root mean square (RMS) of the baseline noise [55, 74, 75]. We filtered the signals using a low-pass inverse Chebychev filter with a cut-off frequency of 1 kHz in the Minianalysis software and determined the noise from an area where the recordings showed no detectable events (red box in Supplementary Fig. 1). Next, using the filtered trace, we used automatic detection in Minianalysis software to identify all events. Then each event was manually reviewed. In a subset of cells from WT and Tg2576 mice, we found there were no significant differences in baseline noise between genotypes, either with or without a filter (Supplementary Table 1). All events were checked to be sure there was a rapid rise relative to the decay. The mean frequency and amplitude were calculated for all synaptic events over a 2 min recording period. In a subset of GCs, we evaluated the role of MC input using the cannabinoid type 1 and 2 receptors agonist, WIN55212-2, which reduces MC→GC synaptic transmission [76].

Initially we recorded sEPSCs at -30 mV because of data showing it is appropriate for recording NMDA receptor-mediated EPSCs [77, 78]. To confirm that EPSCs at -30 mV were mediated by NMDA receptors, the AMPA antagonist DNQX (10 μM) was added to the slices. We noticed that in all our experiments blocking AMPA receptors differentially affected the NMDA-mediated sEPSCs in both genotypes (explained further in the Results section; Supplementary Fig. 2), so we decided to include only the AMPA-mediated excitatory events recorded at -70 mV to quantify excitatory synaptic currents (sEPSCs).

For the analysis of frequency distributions, we also included the parameters of skewness and kurtosis, which describe the shape of the distribution. Skewness reflects the symmetry of the distribution, and kurtosis defines how "peaked" the distribution is compared to a normal distribution. We also analyzed the number of values at the peak of the distribution and the proportion (%) of those events (number of values/total number of events in the distribution). Furthermore, we analyzed the area under the curve (AUC) for each distribution. All analyses were performed using Prism (v.10, GraphPad).

#### *Intrinsic properties*

For intrinsic properties, current-clamp recordings were performed, and the different measurements are shown in Fig. 2A. RMP was defined as the intracellular potential adjusted by the value recorded after withdrawing the microelectrode from the cell. To assess input resistance ($R_{in}$), the steady-state voltage responses resulting from sub-threshold depolarizing and hyperpolarizing pulses (-30 pA to + 30 pA in 5–10 pA current steps; 1 s duration) were plotted against the amplitude of current injection and the slope of the linear fit between – 5 pA to -30 pA was used to define $R_{in}$ (Clampfit v. 11.2; Molecular Devices). Time constant (tau; τ) was determined from hyperpolarizing pulses (-20 pA) and defined as the time to reach 63% of the steady-state response. To determine action potential (AP) characteristics, depolarizing current pulses of + 40 to + 150 pA (10 pA steps; 1 s duration) were delivered to elicit an AP close to its threshold in approximately 50% of trials, and a series of APs. We then used the AP analysis tool in Clampfit (pClamp software v11.2, Molecular Devices) to determine the characteristics of the APs. Threshold was defined as the membrane potential at which the AP initiated, using a three-point tangent slope vector to find the position in the initial region where the slope was at or above 10 V/sec. The mean AP peak amplitude was determined as the voltage difference from RMP to the AP peak. The time to the AP peak was the time from the start of the current step to the AP peak. The time to peak from threshold was measured as the period from the AP initiation to the AP peak. Half-width was defined as the period from the AP initiation to the point when the AP reached half of its peak amplitude. AP rising and decay slopes were defined by the maximum dv/dt of each AP phase, and the dv/dt ratio was defined as the ratio of rising/decay slopes. For the frequency-current (F-I) curve, the mean firing frequency of APs generated by the application of depolarizing current steps (up to + 150 pA in 10 pA steps, 1 s duration) was evaluated. To quantify spike frequency adaptation (Supplementary Figs. 4 and 6) we evaluated the time from one AP peak to the next for all the spike pairs in trains of 4 or 6–7 APs. In a subset of cells, we determined intrinsic properties in the presence of glutamatergic and GABA receptor antagonists (DNQX [10 μM], APV [50 μM], Gabazine [20 μM]) to evaluate if synaptic blockade affected intrinsic properties. We also asked if different RMPs affected intrinsic properties for MCs because WT and Tg2576 MC RMPs differed. Therefore, in a subset of WT and Tg2576 MCs with similar RMPs (between – 65 and – 70 mV), we evaluated intrinsic properties and firing (Supplementary Table 4).

### MCs and GCs identification after electrophysiological recordings

After the completion of recordings, slices were immediately placed in a solution of 4% paraformaldehyde (PFA; Sigma-Aldrich) in phosphate buffer (PB; 0.1 M, pH 7.4) and kept in fixative at 4°C for 24–48 h. For biocytin processing, slices were washed in 0.1 M Tris buffer (TB; Sigma-Aldrich) and permeabilized with 1% Triton X-100 (TX, Sigma-Aldrich) in TB with continuous shaking on a rotator at room temperature for 20 min. Then, slices were incubated in a solution with 0.25% TX in TB for 1 h. Afterwards, slices were incubated in streptavidin-cyanine Cy2 conjugate (1:2000, Jackson ImmunoResearch) in 0.25% TX diluted in TB for 48 h at 4°C and protected from light. After this period, slices were washed in TB and exposed to a series of glycerol dilutions (25, 40, 55, 70, 85 and 90%; Sigma-Aldrich), immediately mounted on a 0.1% gelatin-coated slide surrounded by agar (4%) support, coverslipped using a mounting media solution of 0.5% N-propyl gallate (Sigma-Aldrich) and 90% glycerol in $ddH_2O$, and the edges were sealed (CoverGrip, Biotium). Photomicrographs were acquired with a Zeiss LSM 880 laser scanning confocal microscope and Zen 3.0 software (Zeiss), with Plan-Apochromat 10×/0.45 M27 and Plan-Apochromat 20×/0.8 M27 objectives (Zeiss). All images were acquired at 16-bit depth with a frame size of 2048 × 2048 pixels.

### Immunostaining for c-Fos, Aβ and MC axon identification

#### *Perfusion and sectioning*

Mice were euthanized when they were ~1 month-old (33–38 days-old). Mice were anesthetized with isoflurane (Pivetal, Aspen Veterinary Resources), followed by urethane (2.5 g/kg; i.p.), and they were transcardially perfused with ~20 mL of cold saline solution, followed by ~20 mL of cold 4% PFA in 0.1 M PB using a peristaltic pump (Minipuls2, Gilson). The brain was quickly extracted and stored overnight in 4% PFA at 4°C. Afterwards, the left hemisphere was cut in the coronal plane and the right hemisphere was cut in the horizontal plane (50 µm-thick sections; Vibratome 3000, Ted Pella). The coronal and horizontal planes were used to optimize visualization of the sublamina of the DG molecular layer (ML), and in particular the MC axon terminal plexus in the inner molecular layer (IML). Sections were stored in 24-well tissue culture plates containing cryoprotectant solution (30% sucrose, 30% ethylene glycol in 0.1 M PB) at -20°C until use. In all cases, immunofluorescence staining was performed on free floating sections, and quantification was averaged from four horizontal sections, 600 µm apart, per subject.

#### *c-Fos immunostaining*

Sections from WT and Tg2576 mice were processed together. Free-floating sections were washed in 0.1 M TB (3 washes, 10 min each) and subsequently incubated in two different solutions containing 0.25% TX in TB (TrisA), and 1% BSA and 0.25% TX in TB (TrisB), for 15 min each. Then sections were incubated in a blocking solution containing 5% normal goat serum (NGS; S-1000, Vector Laboratories), 1% BSA and 0.25% TX in TB for 60 min at RT. The primary antibody was a rabbit monoclonal anti-c-Fos antibody (Ab190289, Abcam) and was diluted in blocking solution (1:2000). Sections were incubated for 48 h at 4°C with continuous shaking. On the second day, sections were rinsed in TrisA and subsequently in TrisB for 15 min each, then incubated in goat anti-rabbit Alexa Fluor 488 secondary antibody (1:500; A11004, Invitrogen) diluted in TrisB and 3% normal goat serum (NGS; Vector Laboratories), for 2 h at RT, followed by a rinse in 0.1 M TB for 10 min. Next, sections were mounted on 0.1% gelatin-coated slides and allowed to dry for 1–2 h, and coverslipped with an antifade mounting medium containing DAPI (Vectashield HardSet H-1500, Vector Laboratories).

#### *Aβ immunostaining*

For Aβ immunostaining, we used an antibody raised against the N-terminal fragment residues 1–12 of human Aβ (McSA1; MM0015p, Medimabs), which can detect oligomeric and highly aggregated insoluble forms of Aβ, as we previously reported [55]. Sections were treated with an antigen retrieval procedure where initially slices were washed in 0.1 M PB (3 washes, 10 min each), followed by an incubation period of 3 h in 0.1 M PB, pH 7.4, at 60°C to unmask the epitope of interest. Then, sections were rinsed in 0.1 M PB (3 washes, 10 min each) and incubated for 20 min in 0.5% TX diluted in 0.1 M PB, followed by incubation for 2 h in blocking solution containing 5% NGS (Vector Laboratories) and 1.5% Mouse-on-Mouse (MOM) blocking reagent (Vector Laboratories) in 0.1 M PB to block non-specific binding. Subsequently, sections were incubated for 48 h at 4°C in mouse monoclonal primary antibody to McSA1 (1:1000) in 3% NGS and 0.5% TX diluted in 0.1 M PB. On the second day, slices were washed in 0.1 M PB (3 washes, 10 min each) and incubated with goat anti-mouse IgG Alexa Fluor 488 secondary antibody (1:350, A11001, Invitrogen) for 2 h at RT. Finally, sections were rinsed in 0.1 M PB (3 washes, 10 min each), mounted on 0.1% gelatin-coated slides, allowed to dry, and then coverslipped with antifade mounting medium containing DAPI (Vectashield HardSet H-1500, Vector Laboratories).

#### *Calretinin immunostaining*

To better visualize MC axons, we performed immunostaining against calretinin, a MC marker [79, 80]. We proceeded exactly as explained for c-Fos immunostaining but used a primary antibody to calretinin instead of c-Fos (1:2000; mouse anti-calretinin, 6B3, Swant). For calretinin and c-Fos double labelling, the secondary antibodies were chosen against the species of the primary antibody and with different Alexa Fluor color tags (1:500; goat anti-rabbit Alexa Fluor 488, A11004; goat anti-mouse Alexa Fluor 568; A11008, Invitrogen). The rest of the procedures were identical to c-Fos immunostaining.

#### *Image acquisition*

Photomicrographs were acquired with a Zeiss LSM 880 laser scanning confocal microscope and Zen 3.0 software (Zeiss), with Plan-Apochromat 10×/0.45 M27 and Plan-Apochromat 20×/0.8 M27 objectives. All images were acquired at 16-bit depth with a frame size of 2048 × 2048 pixels. For high-resolution insets, the Plan-Apochromat 20×/0.8 M27 objective was used with a 2.4x digital zoom. Immunofluorescence was visualized with preconfigured excitation and emission wavelengths in the acquisition software for DAPI (Ex/EM 408/453 nm), Alexa 488/GFP (Ex/EM 488/535 nm), and Alexa 568/mCherry (Ex/Em 561/643 nm). Zen 3.2 Blue Edition software (Zeiss) was used offline to perform all quantification, as explained below, and to convert raw Zeiss image files (CZI format) into TIF format. The same parameters, including pixel time, gain and offset, were used for every image acquisition.

### Quantification

#### *c-Fos-immunofluorescence (c-Fos-IF)*

c-Fos-IF was quantified by defining two different regions of interest (ROI) encircling the hilus and the GC layer (GCL). The GCL was defined as the area where GC somata are packed together between hilus and the ML, and the hilus was defined as zone 4 of Amaral [60, 73] (Fig. 6A). C-Fos-IF was quantified using Zen 3.2 Blue Edition software (Zeiss) on images acquired at 20x. C-Fos-IF was calculated by subtracting the background from the mean intensity. The background was defined as the average of two different ROIs with no cells (stratum lacunosum-moleculare and the outer third of the ML; OML). C-Fos-IF was normalized and is presented as the percentage of change from background (% of background).

#### *c-Fos + cell quantification*

To quantify the number of c-Fos + cells within each ROI, we used a thresholding method to count only the brightest cells. Cells that were too close to the background were excluded. To define the threshold, we removed the lowest 10% from the range of fluorescence detection. We selected 10% because we found it was very effective in removing those cells close to background in their fluorescence without removing a great deal of the range of fluorescence. We then quantified the number of cells in the range of fluorescence detection. C-Fos + cell bodies were quantified using the "events detection tool" in Zen 3.2 Blue Edition software (Zeiss). From three to four sections were used per mouse, distributed within the same part of the septotemporal axis.

#### *Aβ-immunofluorescence (Aβ-IF)*

Aβ-IF quantification was performed as described for c-Fos-IF, where the two different ROIs including the hilus and the GCL were defined, and the level of Aβ-IF was quantified using Zen 3.2 Blue Edition software (Zeiss) on 20x magnification images. Two different background values were evaluated from two locations without detectable Aβ-IF (in stratum lacunosum-moleculare and the OML) and averaged, which were subtracted from the values of intensity of the analyzed area for each section. Aβ-IF was normalized and presented in the results as the percentage of change from background (% of background).

#### *Quantification of MC axons*

To quantify potential differences between the axons of Tg2576 and WT MCs, calretinin-mCherry + immunofluorescence was evaluated in the IML (Fig. 8). The ML was defined as the region between the fissure and GCL [48, 73] (Fig. 8B, C). The IML, MML, and OML subdivisions of the ML were determined by dividing into equal thirds the total width of the ML, where the IML is closest to the GCL border and the OML ends at the hippocampal fissure. MC axon distribution was quantified in the upper blade (UB, suprapyramidal), crest (also called apex), and lower blade (LB, infrapyramidal) of the DG (Fig. 8B), as previously defined [63].

The distance measurements were performed using the "distance tool" in the Zen 3.2 Blue Edition software (Zeiss). The length feature of the distance tool allows drawing parallel lines between two points to determine the length between them. Thus, one line from the GCL border to the edge of the mCherry + axon terminal plexus (the dense band of mCherry + puncta reflecting MC axon boutons) was drawn, along with one line from the GCL border to the end of the ML (Fig. 8C1a and 8C2b). Distance measurements were normalized as the percentage of the total ML width (% of ML) by dividing our measurement of interest by the total width of the ML. All analyses were done using horizontal sections, and a minimum of three relatively dorsal and three ventral sections were analyzed per mouse and averaged.

### Novel object recognition (NOR) test

The NOR test has been shown to be a hippocampal-dependent task which involves the DG [81, 82]. For this test, mice were acclimated for three consecutive days (5 min each, Supplementary Fig. 8A1), allowing every animal to freely explore a standard rat cage (26 cm wide x 40 cm long x 20 cm high) inside a larger cardboard box with no cover (40 cm wide x 60 cm long x 50 cm high). There were 3 pictures placed on the walls of the box with different shapes (10–20 cm wide, 12–27 cm tall) and a combination of different colors (white, black, green, yellow, red) to provide a consistent context. Each picture was centered on each wall and one edge touched the base of the box. All acclimation, training and testing sessions were performed between 10:00 a.m. – 12:00 p.m., and all equipment was cleaned using 70% ethanol between each session. On day 4, a training and testing session (5 min each) were conducted, with an interval between sessions of 1 h. Video recordings of all training and testing sessions were captured using a mobile phone camera with a 720p resolution and exported as H.264 MPEG-4/AVC videos. During the training session, mice were placed in the testing arena containing two identical objects (2 pineapple-like metal objects, 3 cm diameter x 6 cm height) centered along the shortest cage wall (Supplementary Fig. 8A2) and allowed to explore them for 5 min. Afterwards, the mouse was removed and placed in its home cage for 1 h. For the testing session, one of the objects was replaced with a different one (a glass vial, 3 cm diameter x 6 cm height, filled with pieces of metal and salt to make it heavy; Supplementary Fig. 8A3), and the mice were allowed to explore them for 5 min. Videos of the training and testing sessions were analyzed offline using ANY-maze video tracking system software (v7.3, Stoelting). Exploration was quantified as the time each mice spent exploring the objects, defining exploration as the nose pointed at the object and in a proximity of at least 2 cm of the object, and when animals spent time on top of the object, were looking down and sniffing it. The number of approaches to the object were also quantified. Exploration of the novel object during NOR testing was expected to be higher than 50% (compared to 50% for the training period) of the total time of object exploration, as this reflects animals can remember the objects seen in training (Supplementary Figs. 8B and 9B). In a subset of experiments, the novel object location (NOL) task was performed. The procedure was the same as described for NOR, but instead of introducing a novel object, one of the two objects in the testing box was changed to a different position. Estimation of time exploring this object was the same as explained for NOR.

### Statistics

All statistical analyses were performed using Prism software (v.10, GraphPad). For data that were normally distributed determined by the Shapiro-Wilk tests, parametric statistics were used. Otherwise, non-parametric tests were applied. For pairwise comparisons, homogeneity of variance was evaluated using the F test, and to compare multiple groups the Brown-Forsythe test or Bartlett's test was used.

For parametric data, statistical significance between two groups was determined using the unpaired Student's t-test, which was also used for data at two time points during the same event (e.g., train of APs). For non-parametric data, a Mann-Whitney *U* test was used for paired comparisons.

Because frequency distributions were not normal, a non-parametric test, Friedman's two-way ANOVA by Ranks test, was used to compare frequency distributions of WT and Tg2576 mice (v.30, SPSS, IBM). The main factors were genotype and bin. Each bin amplitude was a specific range of amplitudes, and each bin range (e.g. 0.1 mV) was identical to the next. In addition, we analyzed the data by identifying every cell and genotype as factors for every bin. These data followed a normal distribution, so a two-way ANOVA was used. To analyze cumulative distributions, we used the Kolmogorov-Smirnov (KS) test. For the frequency and current injected relationship (F-I curve), a linear correlation of the mean firing frequency vs. the current injected was determined, and then the Fisher z-transformation of the Pearson correlation coefficients was used to evaluate statistical differences between groups. A two-way repeated measures (RM) ANOVA (or mixed-effects model) followed by Šídák's post-hoc test for multiple comparisons was used to address the sequential APs of a train with genotype and current injected as factors. The same approach was used for analysis of spike frequency adaptation.

To address sex as a biological variable, two-way ANOVAs were used with sex and genotype as factors. Šídák's post-hoc test for multiple comparisons was used. For the analysis of the MC axon distribution, comparisons between parametric data were performed using unpaired t-tests for two groups and ANOVAs for more than two groups. For non-parametric data, the Mann-Whitney and Kruskal-Wallis tests were used. When we asked whether the septotemporal area had an effect, two-way ANOVAs were used with location and genotype as factors. Šídák's post-hoc test for multiple comparisons was used. For comparing the RMP vs. AP threshold and RMP vs. rheobase, a linear regression analysis was performed, and the slopes were used for statistical comparisons. A comparison of the correlations was also made using the Fisher-Z test.

All results are presented as the mean ± standard error of the mean (SEM), and statistical significance was achieved if the p value was < 0.05 (denoted on all graphs by an asterisk).

## Results

### Comparison of MC synaptic and intrinsic properties in WT and Tg2576 mice

#### *Spontaneous synaptic events*

There were 28 MCs from 22 Tg2576 mice and 28 MCs from 18 WT mice. For GCs, there were 25 cells from 16 Tg2576 mice and 24 GCs from 16 WT mice. No more than 3 cells (MCs or GCs) and 2–3 slices were used per mouse.

#### *Spontaneous excitatory synaptic potentials are increased in Tg2576 MCs*

MCs were recorded using the current clamp configuration to assess sEPSPs (Fig. 1A). MCs from Tg2576 mice showed a significantly higher sEPSP mean frequency than WT mice (Tg2576: 8.82 ± 0.93 events/sec, WT: 5.84 ± 0.45; Mann-Whitney test, U = 76, $p = 0.006$; Fig. 1B1, 1B2). There were no differences in MC mean amplitudes (Mann-Whitney test, $p = 0.521$; Fig. 1B2), but the frequency distributions of sEPSP amplitudes showed a larger number of small events in Tg2576 MCs (Fig. 1B3). Further analysis of the frequency distributions is shown in Supplementary Fig. 3. The significant differences in genotypes for frequency distributions (Friedman's two-way ANOVA by Ranks test, test statistic = 21.225; $p < 0.001$) and cumulative distributions (Kolmogorov-Smirnov test, D = 0.117, $p = 0.001$; Fig. 1B4) were consistent with an increase in sEPSPs in Tg2576 MCs. When the frequency distributions were analyzed with cell identity and genotype as factors, there was a significant difference for both factors (two-way ANOVA; cell identity: F (17, 18396) = 5.977; $p < 0.001$; genotype: F (1, 18396) = 15.43; $p < 0.001$; Supplementary Table 2). Taken together, the results suggest that sEPSP frequency of Tg2576 MCs was greater than WT.

#### *Spontaneous excitatory synaptic currents are increased in Tg2576 MCs*

Next, AMPA receptor-mediated sEPSCs were compared in WT and Tg2576 MCs in voltage clamp. The experimental timeline for voltage clamp experiments (Fig. 1A) was analogous to current clamp, but different MCs were recorded due to the use of different intracellular solutions. As we reported [55], AMPA-sEPSCs were identified as fast inward currents at -70 mV holding potential. Tg2576 and WT MCs did not differ significantly in mean frequency (unpaired t-test, $p = 0.755$; Fig. 1C) or mean amplitude (unpaired t-test, $p = 0.192$; Fig. 1C). However, Tg2576 MC frequency distributions of amplitudes illustrated a greater number of small events, possibly due to the trend for reduced mean amplitudes, as well as more large events in WT MCs. The greater number of large events in WT MCs is noted by a black arrow in Fig. 1C3 (compared to the red arrow for the Tg2576 MC data). Further analysis of frequency distributions is shown in Supplementary Fig. 3. A Friedman's two-way ANOVA by Ranks test with the genotypes and bin as factors showed genotype was a significant factor (test statistic = 189.777; $p < 0.001$). Cumulative distributions also showed greater AMPA-sEPSCs in Tg2576 MCs (Kolmogorov-Smirnov test, D = 0.365, $p < 0.001$; Fig. 1C4). Interestingly, these results for distributions were not consistent with the lack of difference between means (Fig. 1C), which could be due to the fact that all events are pooled to determine the mean, but they are separated when plotting the distributions, making distributions more sensitive. When the frequency distributions were analyzed with cell identity and genotype as factors, there was a significant difference for both factors (two-way ANOVA; cell identity: F (8, 8856) = 15.01; $p < 0.001$; genotype: F (1, 8856) = 188.6; $p < 0.001$; Supplementary Table 2). Overall, the data are consistent with a greater number of AMPA-sEPSCs in Tg2576 MCs relative to WT.

Regarding sEPSCs mediated by NMDA receptors, we used a holding potential of -30 mV as others have done before [77, 78]. However, the AMPA receptor antagonist DNQX reduced sEPSCs (Supplementary Fig. 2). Interestingly, DNQX decreased the sEPSC frequency more in WT cells than Tg2576 mice (WT: to 96.33% of baseline values; Tg2576 cells to 49.39%; Supplementary Fig. 2A2). The comparison of frequency before and after DNQX for WT cells was significant (baseline: 1.48 ± 0.32 events/sec; DNQX: 0.05 ± 0.01; Welch's t-test, t = 4.507, df = 2.002, $p = 0.023$) but it was not significant for Tg2576 cells (Welch's t-test, $p = 0.108$; Supplementary Fig. 2A2). Results for sEPSC amplitude were similar: there was a significant reduction in WT sEPSCs (to 34.14% of baseline values) and Tg2576 EPSCs (to 20.16%) and the effects of DNQX in WT mice were significant (baseline: 9.91 ± 0.53 pA; DNQX: 6.52 ± 0.48; unpaired t-test, t = 4.725, df = 4, $p = 0.005$), but they were not in Tg2576 mice (unpaired t-test, $p = 0.104$; Supplementary Fig. 2B2). These data suggest interesting differences in the NMDA-sEPSCs between WT and Tg2576 that are consistent with differences in NMDA-sEPSCs we previously reported [55] and merit further studies.

#### *Spontaneous inhibitory synaptic currents are reduced in Tg2576 MCs*

To assess spontaneous inhibitory synaptic currents (sIPSCs), MCs were the same as those used to record sEPSCs, but they were held at + 10 mV holding potential, where sIPSCs are recorded as fast outward currents

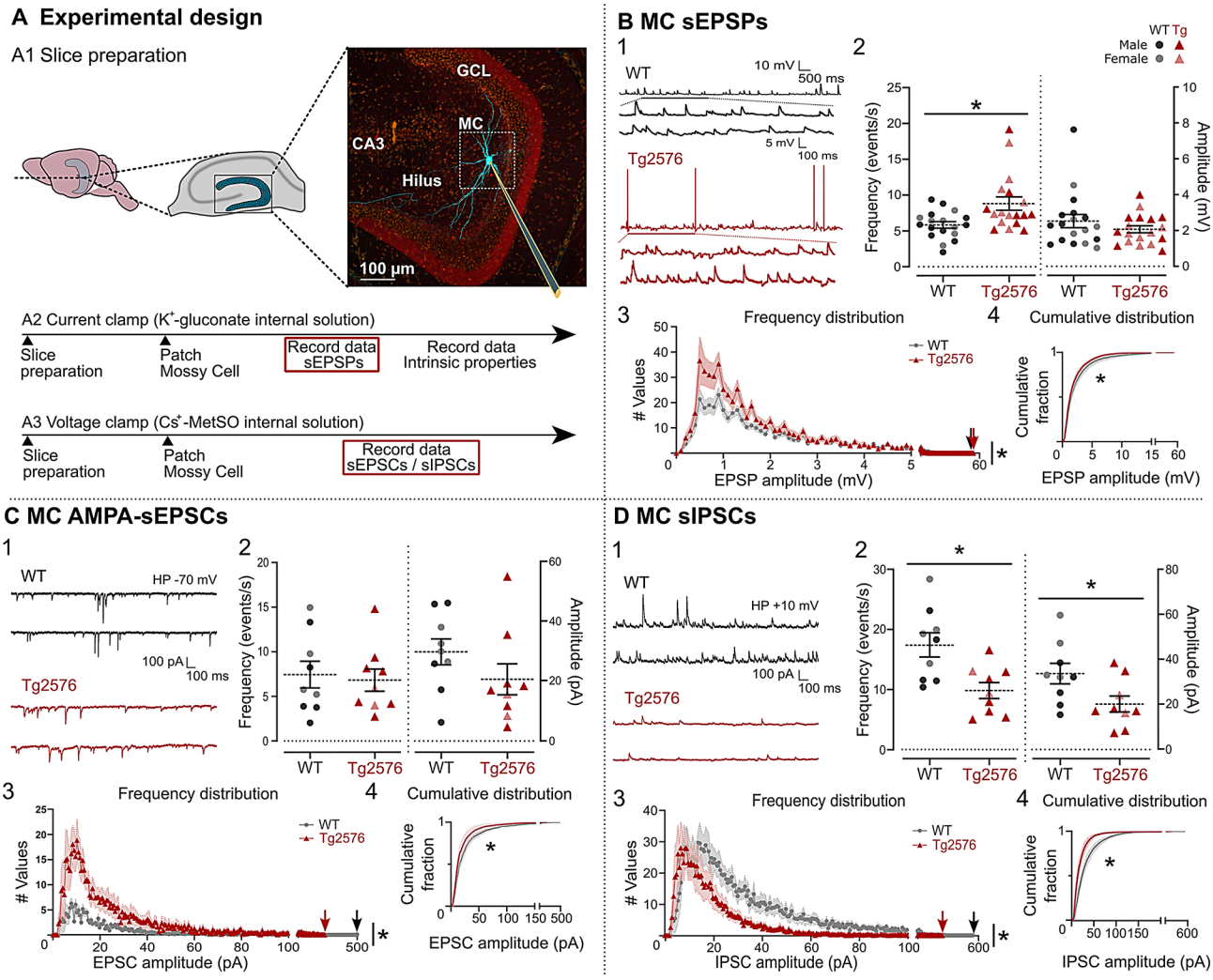


**Fig. 1** Tg2576 MCs exhibit increased excitatory and decreased inhibitory synaptic activity. **(A)** 1. An illustration of the location of the hippocampus (left) and a cross-section through the hippocampus showing the DG (center). On the right is a micrograph of the DG illustrating a MC that was recorded with a biocytin-filled electrode (blue). 2, 3. The timeline of the slice preparation and recordings of spontaneous synaptic activity and intrinsic properties from MCs (2, current cl 3, voltage clamp). **(B)** (1) Representative traces of sEPSPs from WT (black) and Tg2576 mice (red). (2) Quantification of sEPSP frequency showed that mean sEPSP frequency was significantly greater in Tg2576 mice but not mean amplitude. (3) Frequency distributions of sEPSP amplitudes were different in the genotypes. Red and black arrows point to the maximums. (4) The cumulative distributions revealed significant differences between WT and Tg2576 MCs. **C.** (1) Representative traces of AMPA-sEPSCs. (2) There were no significant differences in mean frequency or amplitude. (3) Frequency distributions showed genotype differences with more small events in Tg2576 mice, and more large events in WT mice (compare arrows pointing to the maximums). (4) The cumulative distributions were significantly different in WT and Tg2576 mice, consistent with the frequency distributions. **D.** (1) Representative traces of sIPSCs. (2) There was a significant reduction in mean sIPSC frequency and amplitude in Tg2576 mice. (3) Frequency distributions of events show significant differences. (4) The cumulative distributions revealed significant differences between WT and Tg2576 MCs. For this and all other figures, data are represented as mean ± SEM. *$p < 0.05$. Details of statistical comparisons are in the text and supplemental tables.

(Fig. 1D1). In Tg2576 MCs, sIPSC mean frequency was significantly lower than WT (Tg2576: 9.81 ± 1.33 events/sec, WT: 17.38 ± 2.01; unpaired t-test, t = 3.145, df = 16, $p = 0.006$; Fig. 1D2). Furthermore, there was a significant reduction in sIPSC mean amplitude (Tg2576: 20.04 ± 3.57 pA, WT: 33.57 ± 4.56; unpaired t-test, t = 2.337, df = 16, $p = 0.033$; Fig. 1D2). The frequency distribution of sIPSC amplitudes in Tg2576 MCs showed a reduced number of events (Fig. 1D3). A Friedman's two-way ANOVA by Ranks test with the genotypes and bin as factors showed genotype was a significant factor (test statistic = 203.834; $p < 0.001$). Cumulative distributions also showed reduced sIPSCs in Tg2576 MCs (Kolmogorov-Smirnov test, D = 0.084, $p = 0.020$; Fig. 1D4). Furthermore, when frequency distributions were analyzed with cell identity and genotype as factors, there was a significant difference for both factors (two-way ANOVA; cell identity: F (8, 9180) = 8.172; $p < 0.001$; genotype: F (1, 9180) = 94.08; $p < 0.001$; Supplementary Table 2).

Taken together, data from current- and voltage-clamp suggest excitation was increased in Tg2576 MCs, probably because of an increase in small sEPSP/AMPA-sEPSCs in Tg2576 mice, and a reduced number of large sEPSCs compared with WT. Furthermore, there was a significant decrease in sIPSCs of Tg2576 MCs. Therefore, the data suggests an increased E/I balance in Tg2576 MCs, which could contribute to a very early increase in MC excitability in Tg2576 mice.

#### *MC intrinsic properties in Tg2576 mice reflect enhanced excitability*

MC intrinsic properties were examined to determine whether MCs are intrinsically more excitable in Tg2576 mice. We evaluated RMP, $R_{in}$, tau, and characteristics of APs. The AP characteristics were amplitude, measurements of duration (time to peak, half-width), threshold, maximum rate of rise, maximum rate of decay, dv/dt ratio (maximum rate of rise / maximum rate of decay), and rheobase (see Methods and Fig. 2A).

The RMPs were more depolarized in Tg2576 MCs relative to WT (-59.70 ± 1.85 mV vs. -71.66 ± 1.33, respectively; unpaired t-test, t = 5.197, df = 31, $p < 0.001$; Fig. 2C1). Tau was shorter in Tg2576 MCs than WT (39.81 ± 3.69 msec vs. 51.14 ± 3.74, respectively; unpaired t-test, t = 2.142, df = 26, $p = 0.042$; Fig. 2C2). Representative APs at threshold and their phase plots are shown in Fig. 2B. Tg2576 MCs showed a significant reduction in the amount of current necessary to elicit an AP, or rheobase, in comparison with WT MCs (54.55 ± 7.67 pA vs. 115.8 ± 22.75, respectively; Mann-Whitney test, U = 18, $p = 0.002$; Fig. 2C3). AP amplitude was reduced in Tg2576 MCs relative to WT (79.57 ± 3.86 mV vs. 93.50 ± 3.67, respectively; unpaired t-test, t = 2.731, df = 21, $p = 0.013$; Fig. 2C4). The time to the AP peak was shorter in Tg2576 MCs than WT (329.20 ± 58.30 msec vs. 531.50 ± 53.30; unpaired t-test, t = 2.565, df = 21, $p = 0.018$; Fig. 2C5), suggesting Tg2576 MCs fire more easily than WT. Finally, Tg2576 MC APs had a slower maximum rising slope than WT (113.00 ± 14.36 mV/msec vs. 163.20 ± 17.70; unpaired t-test, t = 2.175, df = 21, $p = 0.041$; Fig. 2C6). Tg2576 MCs did not differ from WT in $R_{in}$, threshold, time to peak from threshold, half-width, maximum rate of decay and the dv/dt ratio (Supplementary Table 3).

#### *Tg2576 MCs exhibit enhanced firing behavior*

To assess firing behavior, we evaluated MC AP firing induced by current injection (representative traces in Fig. 3A). The relationship between mean firing frequency and injected current (F-I curve) is shown in Fig. 3B1. In comparison with WT, Tg2576 MCs fired more APs for any injected current step, which is depicted in the separation of the two genotypes by linear regression. These differences were significant when comparing the correlation factor for both genotypes (Fisher z-value for Tg2576 and WT, rz = 2.417 and 1.487, respectively; z-score=-2.460). A two-way RMANOVA also showed significant differences in genotype ($F(1,21) = 20.38$; $p < 0.001$). The other main factor, intensity of current, was also significantly different since current was increased sequentially. Thus, Tg2576 MCs were more inherently excitable compared with WT. To determine if differences in RMP contributed to the results, RMP was plotted in relation to rheobase or AP threshold and correlations were not significant (rheobase: F = 0.469, DFn = 1, DFd = 20, $p = 0.502$; threshold: F = 0.040, DFn = 1, DFd = 20, $p = 0.843$).

We also evaluated spike frequency adaptation in both genotypes (Supplementary Fig. 4). To quantify adaptation, the interspike intervals (measured as the time from one AP peak to the next, or peak to peak time) were compared with trains of 4 APs (3 spike-pairs, SP; Supplementary Fig. 4A) or longer AP trains (6 SPs; Supplementary Fig. 4B). In general, MCs from Tg2576 and WT mice seemed to have weak adaptation, because there were similar interspike intervals during the train. A two-way RMANOVA showed no genotype effect for the 3 AP train ($p = 0.119$) and 6 AP train ($p = 0.769$; Supplementary Fig. 4A1, 4B1). We did not find any significant effect of genotype when the first and third SP were compared in each of the trains with 3 SPs for Tg2576 and WT MCs ($p = 0.791$ and $p = 0.999$, Šídák's multiple comparisons test, respectively), or when we compared the first and sixth SP using longer trains ($p = 0.933$ and $p > 0.999$, Šídák's multiple comparisons test, respectively).

In a subset of MCs with RMPs between −65 and −70 mV (WT: -68.97 ± 0.76; Tg2576: -68.20 ± 1.13 mV; unpaired t-test, $p = 0.570$) we first compared intrinsic properties and found that indeed they did not differ significantly (Supplementary Table 4). Then we analyzed firing behavior and found that genotype was a significant factor (two-way ANOVA, $F(1,8) = 5.834$; $p = 0.042$) with Tg2576 MCs still firing more than WT MCs (Tukey's multiple comparisons test; Supplementary Fig. 5). A Fisher Z test also showed genotypes were significantly different in firing behavior (z score=-2.069). Therefore, differences in RMPs were unlikely to contribute to increased mean firing frequency of Tg2576 MCs.

#### *Tg2576 MCs have an increased E/I ratio*

The E/I ratio of Tg2576 MCs was significantly different from WT for frequency (WT: 0.41 ± 0.06 events/sec; Tg2576: 0.77 ± 0.16; unpaired t-test, t = 2.149, df = 16; $p = 0.047$), but not for amplitude (unpaired t-test; $p = 0.514$; Fig. 4A1, 4A2). When we analyzed the charge transfer of excitatory and inhibitory events, there were no significant differences for sEPSCs (Mann-Whitney test; $p = 0.605$; Fig. 4B1), but a significant reduction in Tg2576 sIPSCs (WT: $9.14 \pm 2.22 \times 10^5$ pA*msec; Tg2576:

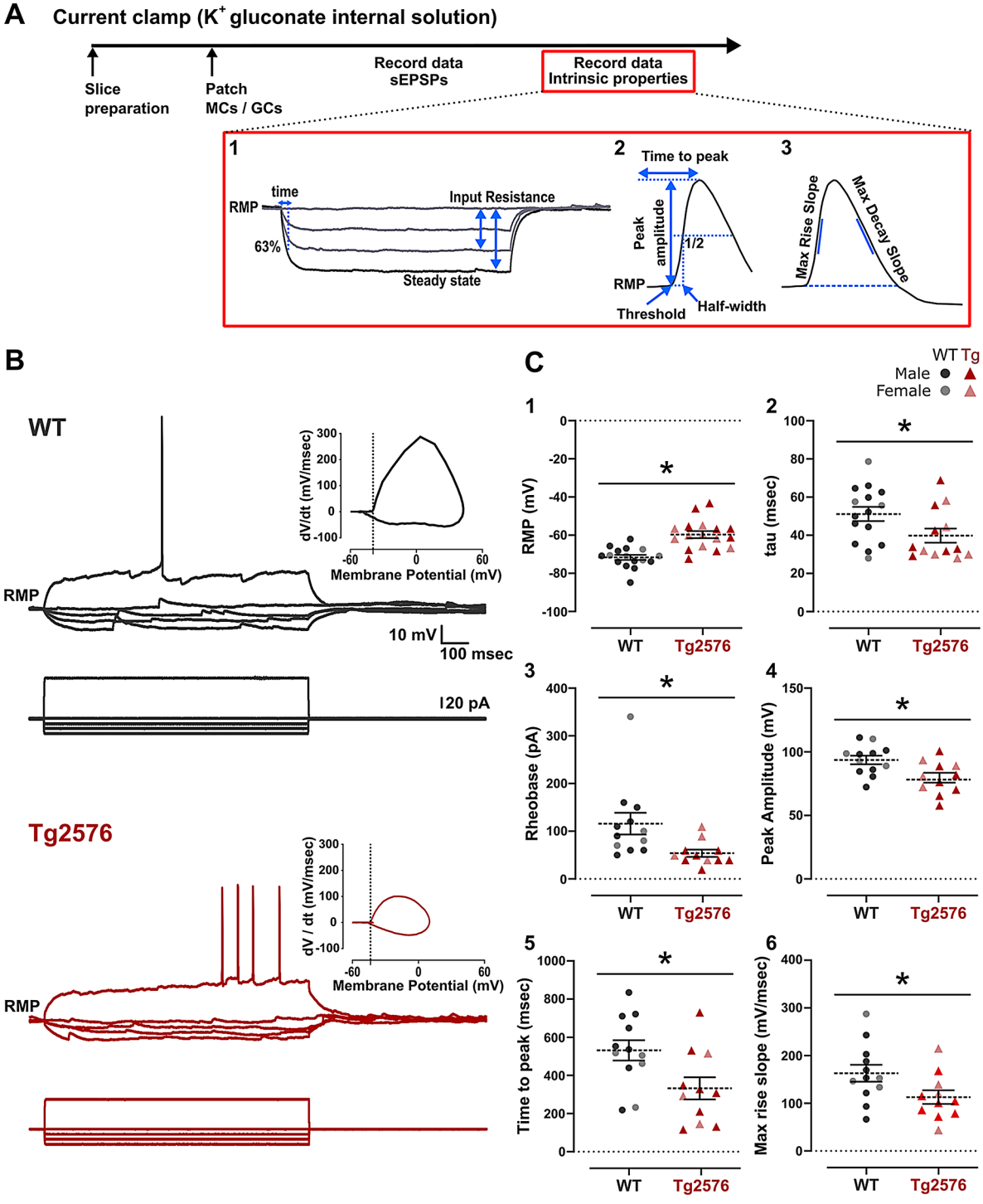


**Fig. 2** MC intrinsic properties of Tg2576 MCs suggest altered excitability. **A.** The timeline of the recordings for the analysis of MC intrinsic properties. 1. Measurements from responses to hyperpolarizing current steps. 2–3. Measurements of APs. **B.** Representative traces of membrane potential responses from WT (black) and Tg2576 MCs (red) to a positive (60 and 70 pA, respectively) and consecutive negative current steps from − 10 to -30 pA using a 10 pA increment. The AP phase plot is shown in the inset. **C.** (1) RMPs were significantly more depolarized in Tg2576 than WT MCs. (2) The time constant was significantly shorter in Tg2576 MCs. 3–4. Rheobase (3) and the time to peak of the AP (4) were significantly reduced in Tg2576 MCs. The data in 1–4 suggest enhanced excitability of Tg2576 MCs. 5–6. AP peak amplitude (5) and maximum rising slope (6) were significantly reduced in Tg2576 MCs. While the data in 1–4 suggest increased excitability, data in 5–6 would potentially decrease excitability

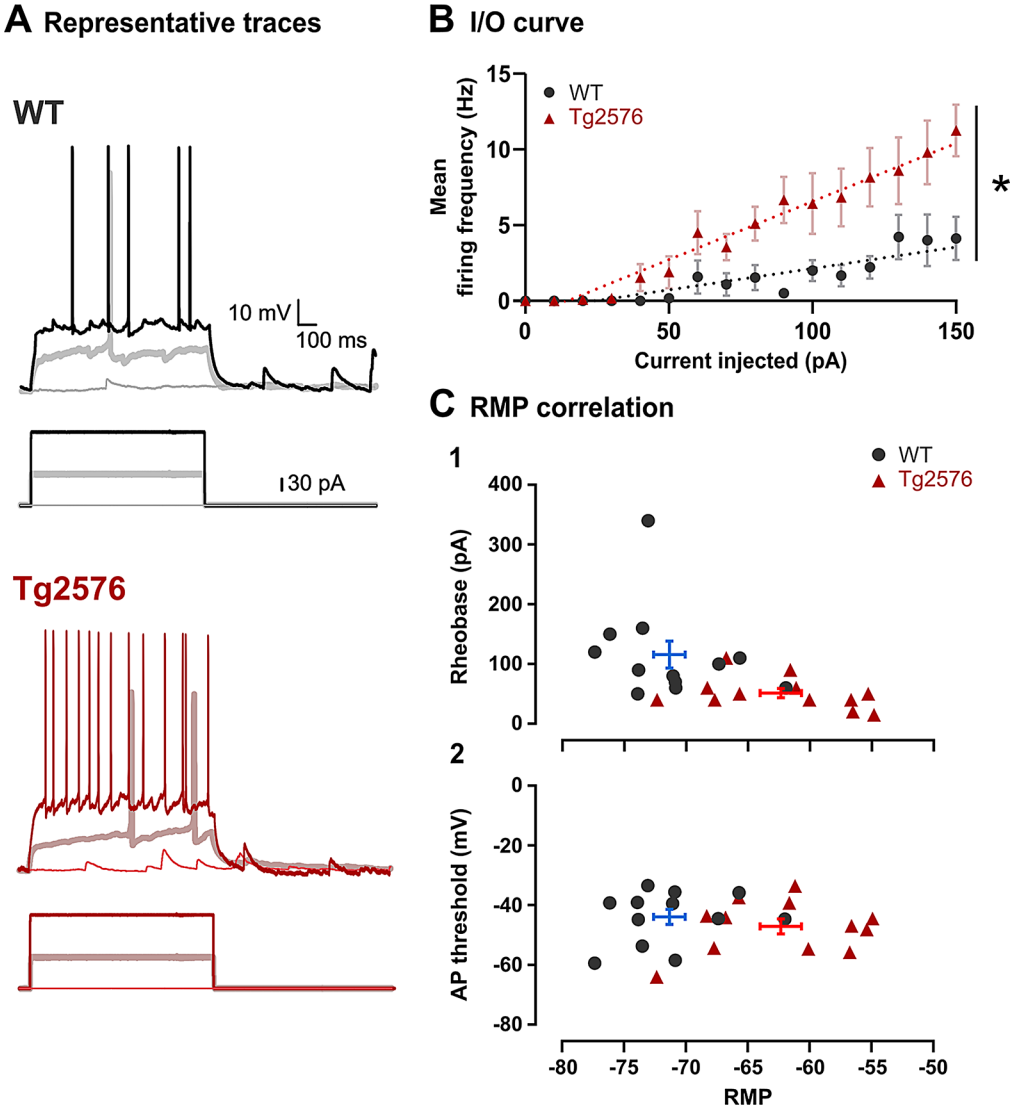


**Fig. 3** Firing behavior of WT and Tg2576 MCs. **(A)** Representative traces show the response of WT and Tg2576 MCs to current steps of low and high amplitude eliciting few and larger numbers of APs, respectively. **(B)** Quantification of the mean firing frequency in response to current steps showed Tg2576 MCs generated a higher mean firing frequency than WT MCs (asterisk, $p < 0.05$). **(C)** (1) A plot of MC RMP vs. rheobase of the same cell for WT and Tg2576 MCs. Means and SEMs are indicated by the blue and red bars. There were no significant differences. (2) A plot of MC RMP vs. the AP threshold of the same cell shows no significant difference between genotypes. The data in C1 and C2 suggest that the relatively depolarized RMPs of Tg2576 mice did not affect rheobase or AP threshold significantly

$3.19 \pm 0.84 \times 10^5$; Welch's test, t = 2.507, df = 10.21, $p = 0.031$; Fig. 4B3). However, the estimation of the E/I ratio based on these values did not show any significant difference in Tg2576 mice compared to WT mice (Mann-Whitney test; $p = 0.136$; Fig. 4B5).

Taken together, the data suggest a very early increased excitability of Tg2576 MCs. The increased excitability is likely to be due to increased sEPSPs/Cs, decreased sIPSCs, and altered intrinsic properties.

#### *Comparison of sex in WT and Tg2576 MCs*

Female and male mice were compared for all measurements described above. However, females were studied without knowing the stage of their estrous cycle. Therefore, the combination of physiological changes dependent on different cycle stages were likely to be underrepresented. We did not find any significant sex differences (Supplementary Tables 5, 6).

### GC synaptic and intrinsic properties in WT and Tg2576 mice

#### *Excitatory and inhibitory synaptic events are increased in frequency in Tg2576 GCs*

Synaptic events and intrinsic properties were compared in WT and Tg2576 GCs following the same protocol described for MCs (Fig. 5A). Tg2576 GC sEPSPs

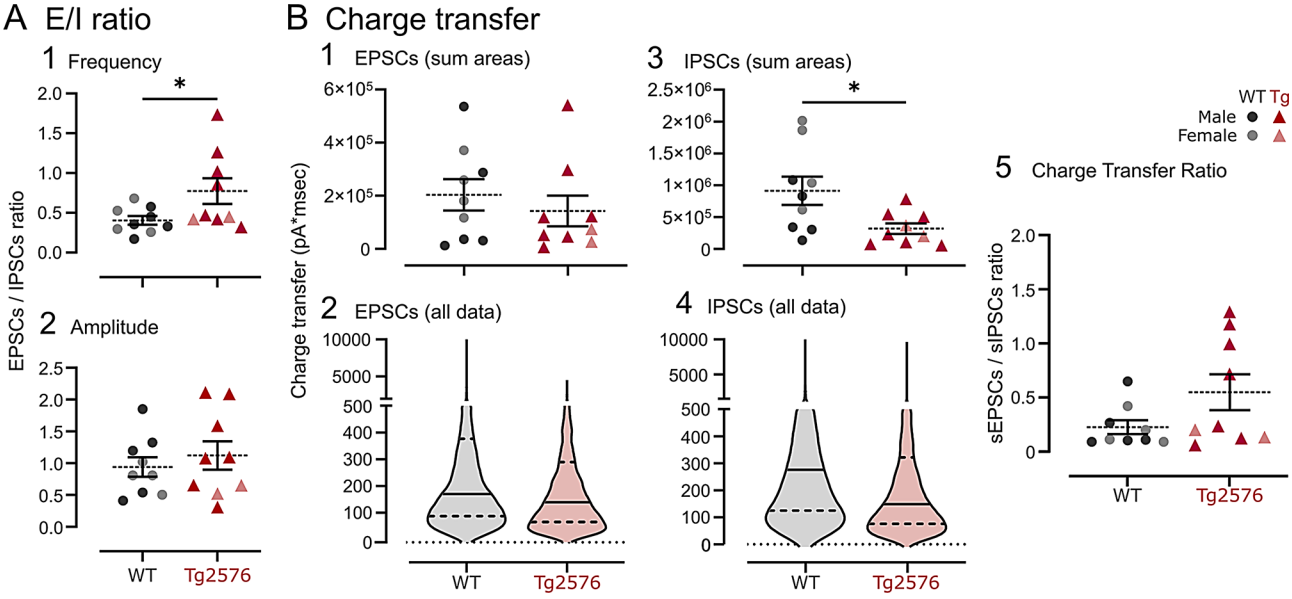


**Fig. 4** Tg2576 MC E/I balance suggests increased excitability. **(A)** Increased E/I ratio in Tg2576 MCs compared to WT MCs. The ratio of sEPSCs (AMPA-sEPSCs) to sIPSCs was increased for Tg2576 MCs based on mean frequency (1) but not mean amplitude (2). **(B)** 1–2. Charge transfer of excitatory currents (AMPA-sEPSCs) based on the sum of event areas (1) or all values (2). 3–4. Charge transfer of inhibitory currents (sIPSCs) was significantly different between genotypes. 5. The E/I ratio for charge transfer based on mean values showed Tg2576 MCs had a slightly increased charge transfer ratio but it was not significant

were similar to WT (frequency: Mann-Whitney test, $p = 0.487$; amplitude: unpaired t-test, $p = 0.996$; Fig. 5B2), which is consistent with no differences in the frequency distributions (Friedman's two-way ANOVA by Ranks; test statistic = 0.947, $p = 0.330$; Fig. 5B3). However, the cumulative distribution was different (Kolmogorov-Smirnov test, D = 0.625; $p < 0.001$; Fig. 5B4). Furthermore, Tg2576 GCs showed a significantly higher frequency of AMPA-sEPSCs (WT: 1.86 ± 0.15 events/sec; Tg2576: 2.53 ± 0.23; unpaired t-test, t = 2.403, df = 31, $p = 0.022$; Fig. 5C2) and sIPSCs (WT: 8.79 ± 0.91 events/sec; Tg2576: 14.24 ± 1.43; Mann-Whitney test, U = 48, $p = 0.001$; Fig. 5D2). When considering genotype as factor, the frequency distribution of AMPA-sEPSCs differed (Friedman's two-way ANOVA by Ranks; test statistic = 7.247, $p = 0.007$; Fig. 5C3), similar to their cumulative distribution (Kolmogorov-Smirnov test, D = 0.210; $p = 0.001$; Fig. 5C4). sIPSC frequency distribution differed when considering genotype as factor (Friedman's two-way ANOVA by Ranks; test statistic = 54.961, $p < 0.001$; Fig. 5D3), as did the cumulative distributions (Kolmogorov-Smirnov test, D = 0.126; $p = 0.011$; Fig. 5D4). Further analysis of frequency distributions is shown in Supplementary Table 7. These data suggest that the presynaptic inputs to Tg2576 GCs may be enhanced, and MCs may play a role as they can excite GCs directly and inhibit them indirectly by exciting interneurons [60, 63]. Therefore, increased MC excitability would increase sEPSCs and sIPSCs to GCs.

***No changes in GC intrinsic properties or firing behavior occur at very early ages in Tg2576 mice***

Tg2576 GC intrinsic properties showed differences from WT at 2–3 months of age [55], but not at 1 month of age (Supplementary Table 8). To confirm changes in synaptic events at 1 month of age did not obscure a change in intrinsic properties, intrinsic properties were reassessed in the presence of glutamatergic and GABA receptor antagonists (DNQX [10 μM], APV [50 μM], Gabazine [20 μM]). The results confirmed that GC intrinsic properties were not changed: there were no differences in genotypes before or after blockade of synaptic transmission (Supplementary Table 9).

In comparison with WT, Tg2576 GCs did not have any significant difference in firing frequency (two-way ANOVA, $p = 0.172$; Supplementary Fig. 6A). Thus, the correlations for the two genotypes showed no significant differences (Fisher z-value for Tg2576 and WT, rz = 2.247 and 2.359, respectively, z-score = 0.297; Supplementary Fig. 6A).

When we compared the interval between SPs for short and long trains, Tg2576 GCs did not differ from WT mice (two-way RMANOVAs, $p = 0.515$ for 3 SPs, and $p = 0.060$ for 6 SPs; Supplementary Fig. 6B1, 6C1). When the first and sixth SPs were examined specifically in the longer AP trains, we found significant differences in GCs, suggesting adaptation occurred (WT: paired t-test, t = 4.229, df = 7, $p = 0.004$; Tg2576: Wilcoxon test, W = 21, $p = 0.031$; Supplementary Fig. 6C2), but there were no differences between genotypes (unpaired t-test; $p = 0.223$, for SP1,

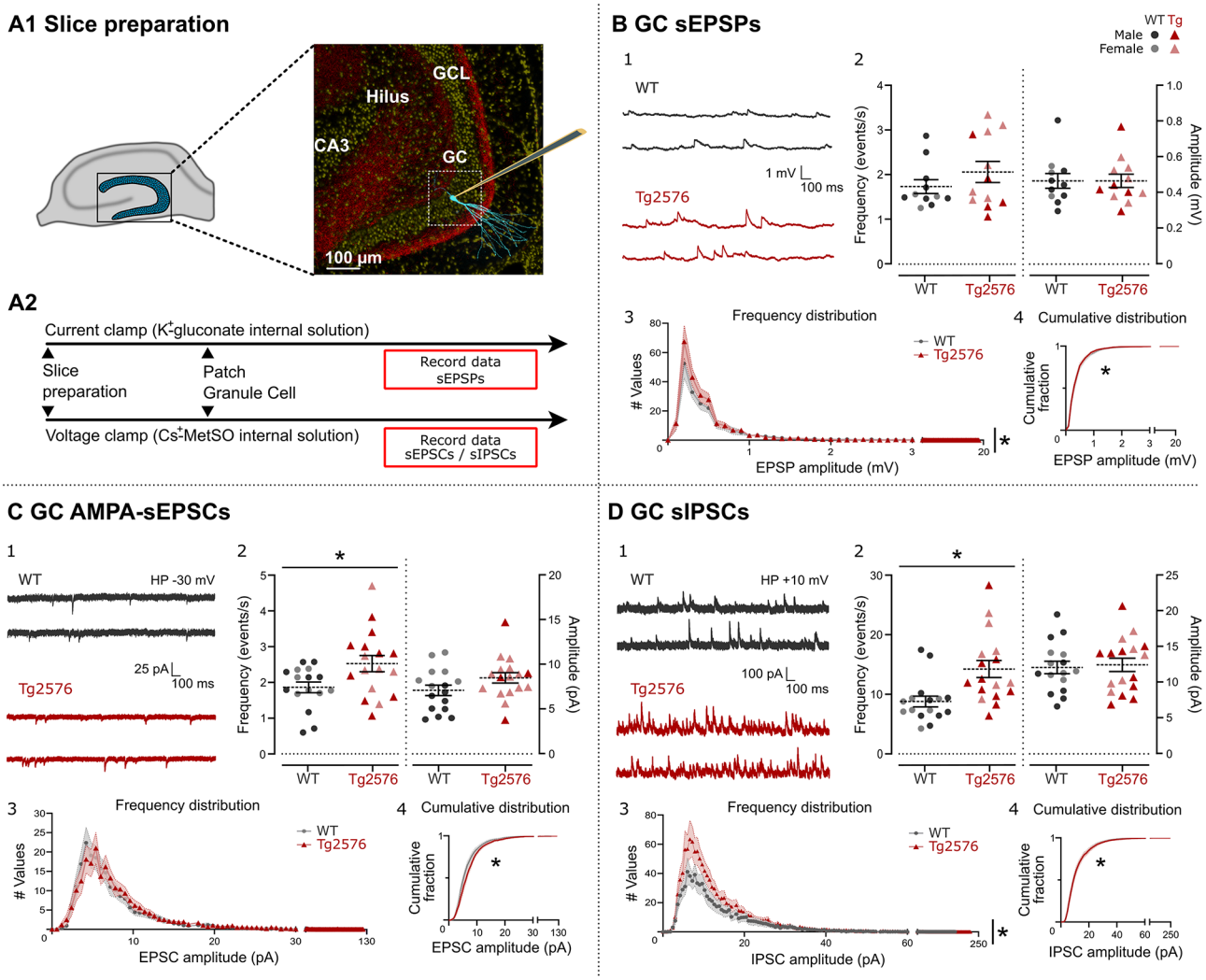


**Fig. 5** Increased spontaneous excitatory and inhibitory events in Tg2576 GCs. **(A)** The timeline of the slice preparation and the electrophysiological recordings for spontaneous synaptic activity in GCs, which was analogous to MCs. A biocytin-filled GC (blue) is shown. **(B)** GC EPSPs. (1) Representative traces of sEPSPs from WT (black) and Tg2576 mice (red). (2) Tg2576 GCs did not show a significant change in mean frequency nor amplitudes. (3) The frequency and cumulative distributions showed significant differences. **C.** GC AMPA-EPSCs. (1) Representative traces of AMPA-sEPSCs from WT (black) and Tg2576 mice (red). (2) Tg2576 GCs had a higher frequency of sEPSCs but not amplitudes. (3) The frequency and cumulative distributions showed significant differences. **D**. GC sIPSCs. Representative traces of GC sIPSCs showed increased frequency but not amplitude of Tg2576 GCs. 3. Frequency distributions of sIPSCs amplitudes showed more small events in Tg2576 mice. (4) Cumulative distributions were significantly different

and Mann-Whitney test; $p = 0.114$, for SP6; Supplementary Fig. 6C2).

### *Tg2576 GCs have a reduced E/I ratio*

Although there was increased excitation and increased inhibition in GCs, we found a significant reduction in the Tg2576 E/I ratio for frequency ($0.16 \pm 0.02$ for Tg2576 and $0.24 \pm 0.03$ for WT; unpaired t-test, $t = 2.449$, $df = 24$, $p = 0.022$; Supplementary Fig. 7A1), although not amplitude (unpaired t-test; $p = 0.265$; Supplementary Fig. 7A2). The charge transfer for excitatory and inhibitory events did not show differences between genotypes (unpaired t-test; $p = 0.142$; and Mann-Whitney test; $p = 0.101$, respectively; Supplementary Fig. 7B1, 7B2), but the E/I ratio using these charge transfer values did show a reduction for Tg2576 GCs ($0.08 \pm 0.01$ for Tg2576 and $0.16 \pm 0.03$ for WT; Mann-Whitney test, $U = 35$, $p = 0.019$; Supplementary Fig. 7B3). Thus, these data suggest GCs at 1 month of age have a reduced E/I ratio but it is a small effect.

### *Sex differences in WT and Tg2576 GCs*

No significant differences were found between WT and Tg2576 male and female mice in the sEPSP, AMPA-sEPSC, or sIPSC frequency or amplitude but AMPA-sEPSCs were greater in WT females than males (Šídák's multiple comparisons test, $p = 0.025$) and Tg2576 females had greater IPSC frequencies than Tg2576 males (Šídák's

multiple comparisons test, $p = 0.030$; Supplementary Table 10).

Interestingly, although we did not find any significant differences when we evaluated GC intrinsic properties with sexes pooled, when separating them by sex we did (Supplementary Table 11). However, the only difference in both sex and genotype was that Tg2576 males had a larger half-width than WT males (Šídák's multiple comparisons test, $p < 0.001$).

#### *Targeting MCs can reduce abnormalities in Tg2576 GCs*

To determine if increased excitability of Tg2576 MCs contributed to increased sEPSCs of Tg2576 GCs, slices were exposed to an antagonist of MC→GC synapses, WIN55212-2 (10 μM). The results showed that WIN55212-2 reduced excitation of GCs to the levels of WT mice. Thus, WIN55212-2 decreased Tg2576 GC sEPSC frequency (baseline: 3.05 ± 0.23 events/sec, WIN55212-2: 2.07 ± 0.34; paired t-test, t = 4.339, df = 5; $p = 0.007$; Supplementary Fig. 8) so it was not significantly different from WT mice (WT baseline: 2.22 ± 0.23 events/sec, Tg2576 after WIN55212-2: 2.07 ± 0.34; unpaired t-test; $p = 0.787$). These findings suggest that MCs and cannabinoid receptor modulators could reduce GC excitation and potentially normalize DG function, which could have translational implications.

### Immunohistochemical analysis of c-Fos-IF and c-Fos + MCs

#### *Increased c-Fos protein expression in Tg2576 hilar cells*

To validate the results regarding the increased activity of Tg2576 MCs in slices, we evaluated the expression of a commonly used marker of neuronal activity, c-Fos (Fig. 6), using similar methods to past studies [82–85].

Our results showed that there was a significantly greater c-Fos-IF in the DG of Tg2576 mice relative to WT (Fig. 6). The hilar area of Tg2576 mice, where MCs are located, had a significant increase in c-Fos-IF (49.75 ± 8.86% vs. 24.65 ± 5.59; unpaired t-test, t = 2.279, df = 9; $p = 0.048$; Fig. 6A2, 6B). Similarly, the Tg2576 GCL had greater c-Fos-IF than WT (68.05 ± 5.68% vs.

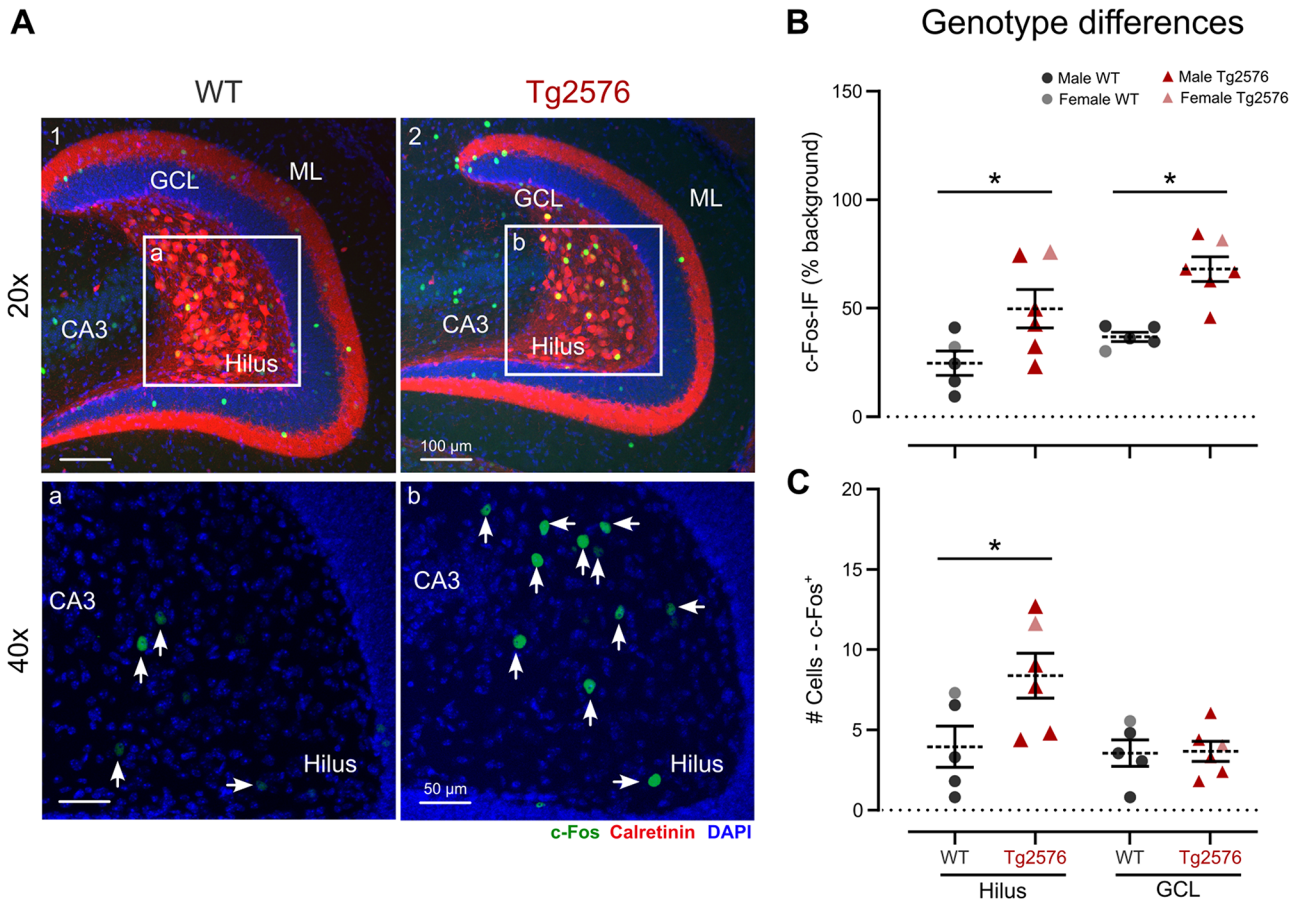


**Fig. 6** Increased c-Fos expression in the DG of Tg2576 mice suggests enhanced neuronal activity. **A.** Micrographs of horizontal sections from WT (1) and Tg2576 (2) DG showing immunofluorescence (IF) for c-Fos protein (green), calretinin (red) and DAPI (blue) in the hilus, granule cell layer (GCL), molecular layer (ML) and CA3. The boxed areas are expanded below and show hilar cells expressing c-Fos (green) that were counted based on thresholding. Arrows point to hilar cells considered immunolabeled. **B.** Quantification of c-Fos IF showed increased expression in Tg2576 hilus and GCL. **C.** There were significantly more c-Fos + hilar cells in Tg2576 mice than WT mice. No significant differences were found for the number of GCs

36.79 ± 2.16; unpaired t-test, t = 4.751, df = 9; $p = 0.001$; Fig. 6A2, 6B). This increased expression suggests enhanced neuronal activity of the cells located in those areas.

### *Increased numbers of c-Fos + MCs correlate with the increased excitability in Tg2576 mice*

In order to know whether the number of cells that expressed c-Fos protein differed between genotypes, we counted the number of bright cells using a threshold. We set threshold at a percentage of the maximum IF so that the brightest cells were easily distinguished from background (see insets in Figs. 6A1, 6A2). The results showed significantly more c-Fos + cells in the hilus of Tg2576 mice relative to WT (8.34 ± 1.40 cells vs. 3.90 ± 1.28; unpaired t-test, t = 2.290, df = 9, $p = 0.048$; Fig. 6C), but not in the GCL (unpaired t-test; $p = 0.915$; Fig. 6C). Thus, there was not only an increased general fluorescence of hilar c-Fos in Tg2576 mice, but also an enhanced number of c-Fos-expressing hilar cells in Tg2576 mice. To determine if the proportion of MCs that were c-Fos + differed between genotypes, 2 sections were selected for each mouse and double labeled using antibodies to c-Fos and a MC marker, calretinin. Sections were chosen from similar septotemporal levels. The total numbers of cells showing double labeling were 69.1% (60/87 cells) of WT mice and 71.6% (43/61 cells) of Tg2576 mice, which was not significantly different (Chi-Square test, $p = 0.843$). These data are consistent with prior studies showing strong c-Fos expression of hilar cells from horizontal sections in mice and rats [82, 83]. They provide additional support for the idea, based on in vitro electrophysiology, that MCs have increased excitability in Tg2576 mice.

### Robust Aβ expression in the hilus of Tg2576 mice

Because we found increased excitability of MCs in slices, we asked if Aβ was expressed in MCs. For this question we used the antibody McSA1, which labels plaques as well as intracellular (soluble) Aβ as we reported before [55]. Representative micrographs of the double labeling of McSA1 and DAPI are presented in Fig. 7A. The McSA1 fluorescence in Tg2576 mice showed that intracellular Aβ was present in hilar cells. We observed there was a very low immunofluorescence in the WT mice. Therefore, Tg2576 mice had significantly greater immunofluorescence (38.00 ± 3.29% vs. 8.74 ± 0.89; unpaired t-test, t = 8.595, df = 6, $p < 0.001$; Fig. 7A2, 7B).

These data suggest that there is a robust and increased amount of soluble oligomeric Aβ at 1 month of age in Tg2576 hilus, which is consistent with our previous

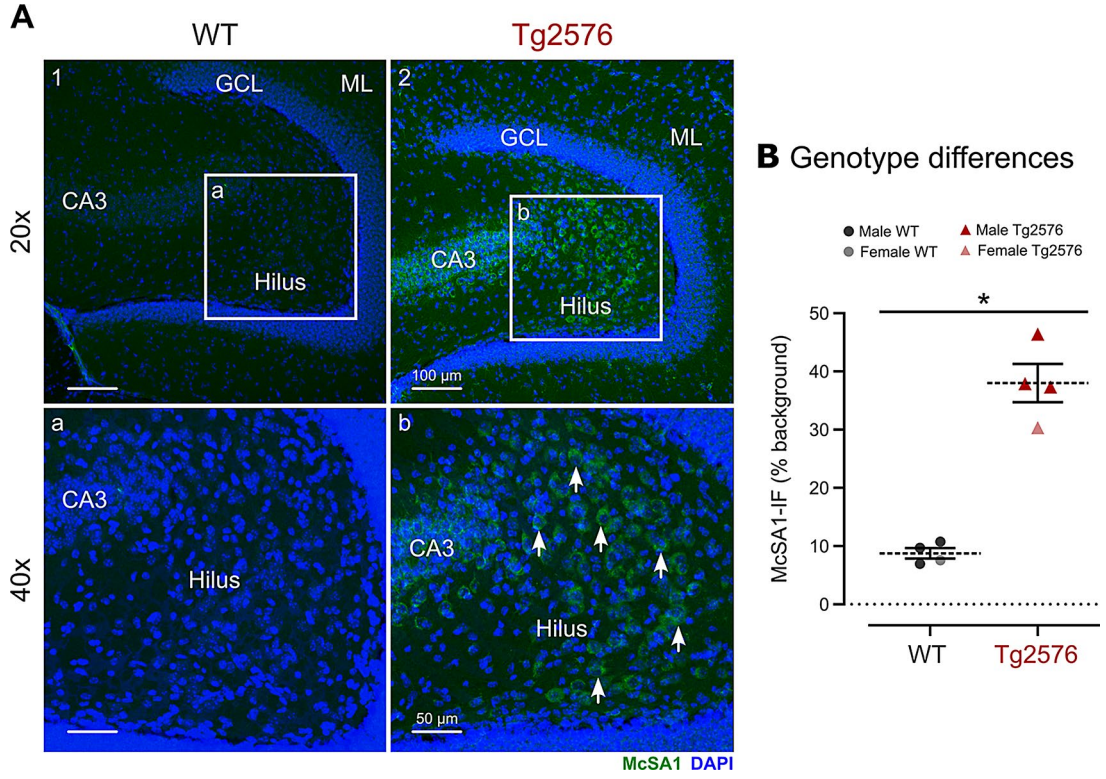


**Fig. 7** Increased Aβ expression in the DG of Tg2576 mice. **(A)** Representative micrographs of immunohistochemical labeling of Aβ with the McSA1 antibody (green) and DAPI (blue) in horizontal sections for WT (1) and Tg2576 mice (2). Images show the hilus, granule cell layer (GCL), molecular layer (ML) and CA3. The boxed areas are shown at higher power below. Hilar cells expressing Aβ are shown in green and pointed with arrows. **(B)** There was significantly more intracellular Aβ labeling with the McSA1 antibody for hilar cells from Tg2576 mice compared to WT

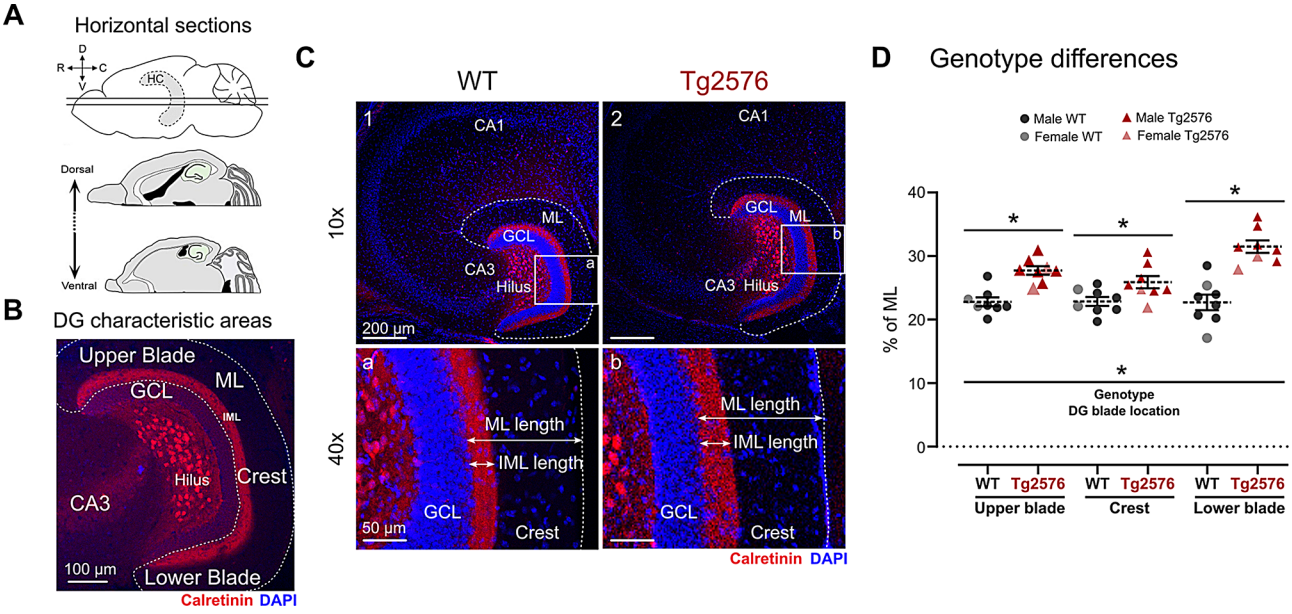


**Fig. 8** MC axons increase in Tg2576 mice. **A.** A diagram shows the plane that was used to generate horizontal sections selected from different parts of the septotemporal axis. **B.** The subregions of the DG are illustrated. Immunofluorescence for calretinin, a marker of MCs, (red) and DAPI (blue), a marker of cell bodies, are shown. **C**. Micrographs of horizontal sections from WT (1) and Tg2576 mice (2). The boxed areas are expanded below and illustrate the measurements of the calretinin-stained MC axon plexus (axon bundle, AB length) and the ML length (horizontal arrows). **D.** Tg2576 mice showed an increase in the calretinin-stained plexus (quantified as the % of the ML)

findings where soluble Aβ levels were elevated at 3 months of age [55, 86]. Therefore, it is possible that the increased excitability of Tg2576 MCs may be due to soluble intracellular Aβ, as has been reported by other studies showing Aβ can lead to altered cellular and synaptic function in other types of neurons [87–95].

## Immunohistochemical identification of the MC axon distribution

### *MC axon distribution in the ML of DG is expanded in Tg2576 mice*

The data described above suggests that one of the reasons GCs may show increased sPSCs in Tg2576 mice was due to increased MC input. Therefore, we asked if there was evidence for more MC input to GC dendrites in Tg2576 mice. To this end we quantified the extent of the axon plexus of MCs in the ML using calretinin to stain MC axons. For quantification, we identified the two edges of the axon plexus: (1) the border with the GCL, and (2) the border with the ML (Fig. 8B and C). We found that in Tg2576 mice, calretinin was a greater percentage of the ML compared with WT in the UB (27.72 ± 0.69% vs. 22.78 ± 0.70, respectively; unpaired t-test, t = 5.122, df = 14, $p < 0.001$; Fig. 8D), crest (25.89 ± 0.97% vs. 22.85 ± 0.70, respectively; unpaired t-test, t = 2.548, df = 14, $p = 0.023$; Fig. 8D), and LB (31.48 ± 0.98% vs. 22.70 ± 1.23, respectively; unpaired t-test, t = 5.582, df = 14, $p < 0.001$; Fig. 8D). Two-way ANOVA revealed a significant main effect of genotype ($F(1,42) = 9678$, $p < 0.001$; Fig. 8D), and also DG blade ($F(2,42) = 5762$, $p < 0.001$; Fig. 8D). Multiple comparisons tests showed significantly more fluorescence in Tg2576 than WT mice in the UB ($p < 0.001$), crest ($p < 0.001$) and LB ($p < 0.001$).

### *MC and GC location was similar for both genotypes*

To confirm cell identity, recorded MCs and GCs were filled with biocytin by diffusion from the patch electrode into the cell (see Methods). A randomly selected group of slices with recorded cells were processed to visualize biocytin (see Methods). An example of a filled MC is shown in Fig. 1A1, and a recorded GC is shown in Fig. 5A. For MCs, we identified them as large (~ 25 µm) cells located in the hilus of DG, with a morphology consistent with a normal adult MC [60]. MC somata were multipolar and had dendrite branches extended throughout the hilar area as previously described [57]. The presence of thorny excrescences was specific for MCs, as previously reported [60, 73].

MCs were sampled from horizontal sections that were divided into relatively dorsal and ventral levels as shown in Fig. 8A. For dorsal sections from WT mice, 13 MCs were sampled, and 3 MCs were close (within ~ 100 µm) to the UB, 5 were close to the crest, 1 MC was close to LB, and 4 MCs were in the middle portion of the hilus (close to the border of the hilus with CA3c). From relatively ventral slices of WT mice, 11 MCs were sampled, and 4 MCs were close to the crest, 3 MCs close to the LB, and 4 MCs in the middle portion of the hilus. For Tg2576

mice, 8 MCs were sampled from relatively dorsal slices, and 1 MC was close to the UB, 1 MC close to the crest, 1 MC close to the LB, and 5 MCs in the middle portion of the hilus. From relatively ventral slices, 17 MCs were sampled, and 3 MCs were close to the UB, 7 MCs close to the crest, 1 MC close to the LB, and 6 MCs in the middle portion of the hilus. In this random sample of MCs, the relative numbers of MCs in dorsal vs. ventral locations were not significantly different between genotypes (Fisher's exact test, $p = 0.156$). The relative numbers of MCs located near the UB, crest, LB, and middle of the hilus were not significantly different for the dorsal WT vs. dorsal Tg2576 mice (Fisher's exact test, $p = 0.504$) or ventral WT vs. ventral Tg2576 mice (Fisher's exact test, $p = 0.329$). Thus, position did not appear to be a contributing factor to increased excitability of Tg2576 MCs.

For GCs, the somata were round or oval, ~10 μm long, and located near the center of GCL, as in our previous study [55]. GCs dendrites extended throughout the ML and contained numerous spines, indicating they were mature GCs [48, 96]. Some GCs were sampled from different portions of the GCL to identify their relative position. For WT, 15 GCs were sampled from relatively dorsal slices, where 4 GCs were in the UB and 11 GCs in the crest. From relatively ventral slices, 8 GCs were sampled, where 1 GC was in the UB and 7 GCs in the crest. For Tg2576 mice, 4 GCs were sampled from relatively dorsal slices, where 1 GC was in the UB, 2 GCs in the crest and 1 GC in the LB. From relatively ventral slices, 18 GCs were sampled, where 2 GCs were in the UB, 7 GCs in the crest and 1 GC in the LB. In this random sample of GCs, there were no significant differences in distributions of GCs in different parts of the GCL (dorsal WT vs. dorsal Tg2576, Fisher's exact test, $p = 0.245$) or ventral WT vs. ventral Tg2576 ($p > 0.999$), suggesting that the location in the GCL could not explain any genotypic differences.

### Behavior

Finally, we asked if increased excitability of MCs influenced behavior of Tg2576 mice at 1 month of age (Supplementary Fig. 9). We chose the NOR test because the DG influences this task [81, 82], we previously showed that NOR is influenced by MCs [97], and NOR was impaired in 3–4 month-old Tg2576 (Supplementary Fig. 10).

The results of the NOR task at 1 month of age are presented in Supplementary Fig. 9. During the training session (Supplementary Fig. 9A, 9B), neither WT (paired t-test; $p = 0.858$) nor Tg2576 mice (paired t-test; $p = 0.247$) showed any preference (exploration time) for one object over the other, i.e., novel object exploration during training approached 50% in both groups (Supplementary Fig. 9B), independent of genotype. This effect was also evident in the discrimination index (Mann-Whitney test; $p = 0.849$; Supplementary Fig. 9C1) where values close to zero suggest no differences in the amount of time the mice explore both objects.

For the NOR testing period (Supplementary Fig. 9A3), the time WT and Tg2576 mice explored the new object was greater than the familiar object (Supplementary Fig. 9B). We observed that Tg2576 ($61.33 \pm 2.92\%$ vs. $50.63 \pm 2.89$ for Test and Train periods, respectively; paired t-test, $t = 2.951$, $df = 4$, $p = 0.042$) and WT mice ($61.15 \pm 1.14\%$ vs. $50.58 \pm 2.99$ for Test and Train periods, respectively; paired t-test, $t = 5.597$, $df = 3$, $p = 0.011$) had a significant % increase of novel object exploration. This same effect was observed in the discrimination index ratio where values different from zero suggest a preference to explore an object (unpaired t-test; $p = 0.989$; Supplementary Fig. 9C2). We also quantified the total exploration time Tg2576 and WT mice spent exploring the new object (unpaired t-test; $p = 0.840$; Supplementary Fig. 9D1) and the number of approaches the mice had to the novel object (unpaired t-test; $p = 0.943$; Supplementary Fig. 9D2). This lack of significant difference between the two groups suggests that Tg2576 and WT mice had novel object recognition memory.

## Discussion

It is known that the DG contributes to increased excitability in hAPP-overexpressing mouse models of AD [16, 23, 24, 31]. Furthermore, DG has been shown to be a critical regulator of hippocampal hyperexcitability in epilepsy research [45, 46, 49, 98]. Increased excitability is important because it has been implicated in the early stages of AD [30]. As the primary cell type and the major output of the DG, the GCs are likely to play a pivotal role. Thus, exploring one of the most important cells that regulate GC activity, the MCs, is highly relevant to early stages of AD.

Our results suggest that by only 1 month of age, there are significant changes to Tg2576 MCs. MCs show increased spontaneous excitatory synaptic events and decreased inhibitory events. Their increased activity is also reflected by depolarized RMPs and increased firing in response to injected current. In support of the in vitro findings, c-Fos protein was increased in MCs of 1 month-old Tg2576 mice. There was elevated Aβ in Tg2576 MCs, suggesting that early accumulation of soluble Aβ may have contributed to MC changes. In GCs, there was already an increased excitatory and inhibitory activity at 1 month of age, and MC input could have contributed because MCs directly excite and indirectly inhibit GCs. Furthermore, an antagonist of MC→GC synapses reduced GC alterations. Additionally, MC axons of Tg2576 mice showed sprouting to the layer where GC dendrites are located, suggesting a reason why MC input to GCs was increased. Together the data suggest that

MCs contribute to early effects in Tg2576 mice, potentially contributing to effects on GCs.

### MCs

Our electrophysiological results suggest that MC excitatory events were greater in Tg2576 mice compared with WT, mainly due to increased frequency, with no significant changes in mean amplitudes. Tg2576 MC inhibitory events (sIPSCs) were significantly reduced in their mean frequency and amplitude. The data suggest that excitatory input to MCs increases, and inhibitory events decrease in Tg2576 mice, increasing excitation and the E/I balance. Our conclusion that Tg2576 MCs had increased excitation relative to WT MCs should be tempered by the differences between current and voltage clamp recordings. Thus, sEPSPs showed increased mean frequency and cumulative distributions in Tg2576 mice, but AMPA-sEPSCs did not, although the frequency and cumulative distributions did. Also, quantification of skewness, kurtosis and other measures of frequency distributions did not capture the same significant differences of sEPSPs and AMPA-sEPSCs. One possible explanation why the data for sEPSPs and AMPA-EPSCs differ is that voltage clamp detects events on distal dendrites better. The idea that voltage clamp would capture more types of inputs than current clamp could also explain the greater variability in AMPA-sEPSCs than sEPSPs (Fig. 1B2 vs. 1C2). The results also are limited to spontaneous events. Nevertheless, the data are novel and potentially significant.

It is unclear at the present time what input is responsible for the increases in sEPSPs and AMPA-sEPSCs in Tg2576 MCs and what inhibitory inputs are reduced in Tg2576 MCs. The excitatory inputs to MCs are mainly from GCs, including semilunar GCs [99] and adult-born GCs [100], which innervate MC proximal dendrites [73]. However, these inputs seem unlikely to be responsible for the effects that we observed because the excitatory events that appeared to increase most were small events, and the GC input to MCs has an unusually large unitary amplitude [63]. Other sources of excitatory input to MCs come from CA3 pyramidal cells [101]. The perforant path activates MC distal dendrites in the ML [102] and there is a monosynaptic pathway from lateral perforant path to MCs [103]. At 1 month of age it has not been shown that the CA3 or perforant path inputs are altered in the Tg2576 mouse, but there is data showing that by 2 months the perforant path input to GCs shows reduced plasticity [54]. By 3–4 months there are measurable defects in the Tg2576 EC [86] and in human AD it has been well documented that the EC shows early vulnerability [104].

MCs also receive input from subcortical areas including serotoninergic, dopaminergic, cholinergic and noradrenergic nuclei [73]. A potential glutamatergic input is from the septofimbrial nucleus [105]. MCs receive GABAergic inputs from DG interneurons in the ML [105] and hilus [64], and possibly extrahippocampal areas [105]. Notably, many defects in subcortical projections and GABAergic neurons have been implicated in AD [31, 106–108], potentially contributing to changes in Tg2576 MCs. Furthermore, there could also be a decline in postsynaptic GABA receptors of Tg2576 MCs since sIPSCs decreased in amplitude.

Our results also show changes in intrinsic properties of MCs in Tg2576 mice, suggesting these cells are intrinsically more excitable (facilitating the generation of APs), and most changes that we found would promote excitability. RMP was more depolarized, τ, rheobase and time to the AP peak were significantly reduced, making MCs more prone to fire APs. We also observed a reduction in the peak amplitude of the APs and in the rising slope in Tg2576 MC APs, which is similar to what has been reported for other cell types in the DG at older ages [108]. The smaller AP amplitudes and slower slopes could be a sign of toxicity due to intracellular Aβ accumulation. Another possibility is that the more depolarized RMP in Tg2576 MCs could have influenced APs due to $Na^+$ channel inactivation. There also could have been compensatory mechanisms to counterbalance the increased MC excitability. Regardless, MC firing behavior showed an enhanced AP firing capacity (F-I curve), as has been shown for other types of hippocampal cells in animal models of AD at older ages [20, 109]. In summary, there was enhanced excitability of MCs in Tg2576 mice at 1 month of age which suggests that they might contribute to the hyperexcitability in GCs during the progression of AD.

### GCs

In contrast to what we found for Tg2576 MCs, we did not find any significant genotypic difference in GC intrinsic properties at 1 month. However, spontaneous synaptic activity, excitatory (sEPSCs) and inhibitory (sIPSCs) inputs to Tg2576 GCs were increased. It is possible that increased excitability of Tg2576 MCs explains the effects on GC synaptic events because MCs directly excite and indirectly inhibit GCs [63, 73]. Thus, more MC activity would potentially explain the increase excitatory and inhibitory inputs to GCs at 1 month of age. The data with WIN55212-2 support that idea, since it reduced GC excitatory events. It also reduced inhibitory events in frequency distributions, but mean frequency and amplitude were relatively unaffected, suggesting a lesser effect on inhibition. The unequal effect of WIN55212-2 may be due to the comparison of a monosynaptic and disynaptic pathway, or fewer cannabinoid receptors at MC→GABAergic neuron synapses.

The lack of differences in GC intrinsic properties at 1 month of age is also notable because our prior study showed intrinsic properties at 3–4 months of age were affected in Tg2576 GCs. One of the changes in Tg2576 GC intrinsic properties at 3–4 months of age was a hyperpolarized RMP compared to WT. Taken together, the present study and previous study suggest that the earliest changes in the progression of pathophysiology are synaptic, not intrinsic. Furthermore, the two studies suggest the intriguing idea that the GC hyperpolarization at 3–4 months might be compensatory. Thus, early in AD there may be compensatory changes that are homeostatic. Then as AD progresses, compensation may no longer maintain homeostasis, leading to the tell-tale symptoms of memory impairment.

#### C-Fos protein expression confirms the increased excitability of MCs in Tg2576 mice and little change in Tg2576 GCs

The conclusion that there was increased excitability of Tg2576 MCs based on in vitro data was supported by enhanced expression of c-Fos protein in Tg2576 MCs. In comparison, GCs showed little effect. However, it is relevant to point out the Tg2576 GCL showed higher c-Fos-IF than WT mice even if the number of c-Fos + GCs was not significantly increased in Tg2576 mice. That result may be due to a greater number of very weakly stained GCs in Tg2576 mice, mostly below the threshold we set for counting c-Fos + cells. The weak staining is interesting because it is consistent with the increased excitatory events of Tg2576 GCs observed in whole-cell recordings. The increased excitatory events might only lead to a small increase in c-Fos protein because sIPSCs also increased.

It is also interesting that other cell types in the Tg2576 mice, like septal neurons, have shown enhanced expression of c-Fos at early ages [23]. The high activity of medial septal neurons is notable because they innervate the DG and could contribute to increased excitability [110–121]. Indeed, the cholinergic input to MCs is robust and might have contributed to synaptic events.

#### Role of Aβ

Our data about enhanced intracellular expression of Aβ in 1 month-old Tg2576 hilar cells may explain why MCs increased excitability, as several studies have documented Aβ-induced enhanced excitatory synaptic mechanisms in hippocampal neurons [87, 89, 91, 95, 122]. However, this conclusion should be made with caution because there is also evidence that Aβ increases inhibition [90, 92, 123–125]. Furthermore, we cannot dismiss the contribution of APP and other APP metabolites besides Aβ, as it has been shown they can influence excitability in AD mouse models [126–129].

#### MC axon distribution differs between Tg2576 and WT mice at 1 month of age

We and others previously showed that axons from dorsal and ventral MCs differ in their projections in normal conditions [62, 130]. Interestingly, our current study shows that there is a thicker MCs axon bundle in the IML of Tg2576 mice. These changes occurred in sections from a large part of the dorsal-ventral axis, suggesting a widespread effect. This small but significant broadening of the MC axon bundle may facilitate an increased functional interaction with GCs, explaining why MCs may contribute to increased synaptic events of GCs independent of the increase in Tg2576 MC excitability. Since MC axons in the ML may also contact GABAergic neurons, the wider axon plexus of Tg2576 MCs may also contribute to increased inhibitory events in GCs of Tg2576 mice. An alternative possibility is that MC axons in ML may interact with other inputs to the ML, like the perforant path input to GCs, because this interaction appears to occur in normal mice [62, 130].

#### Tg2576 mice performance in a memory test is intact at 1 month of age

We previously reported impairment in memory using NOL in Tg2576 mice at ~ 3 months of age [86], which has also been reported in other models of AD at ages older than 3 months [131, 132]. Here we also show that NOR is impaired at that age. To determine if alterations in MCs may impair memory at earlier ages, we chose the NOR test because it involves MCs [97]. Tg2576 mice did not present any difference compared with WT. This is an important result because it shows that alterations at the cellular level occur before memory is affected. That information is useful because it suggests the changes in cells like MCs could be a biomarker. In addition, an intervention that begins as the cellular changes occur might prevent impairments in memory better than an intervention that begins once memory is already impaired.

#### Sex differences

Sex differences in AD have been of great interest, as AD incidence is greater in female than males [133], and females appear to be affected earlier and more severely in animal models of the disease [134–138]. In the present study, we could not find any significant differences in MCs synaptic and intrinsic properties when sex was considered as factor. However, we did observe sex differences which are important to bear in mind as more efforts are made to clarify the role of the DG in AD.

## Conclusions

By using a combination of whole cell electrophysiology and immunohistochemical labeling techniques, this study provided new evidence about the involvement of

MCs in the development of the earliest alterations in the Tg2576 mouse model of AD neuropathology. We propose that these changes, involving the enhanced neuronal activity of MCs and the apparent greater innervation of their postsynaptic targets, are among the very first alterations that occur in the DG of Tg2576 mice that, in the long term, lead to hyperexcitability and the further progression of the pathophysiological process. As such, this study provides insight into potentially new biomarkers and therapeutic targets.

**Abbreviations**

| | |
|---|---|
| AD | Alzheimer's disease |
| Aβ | Amyloid β |
| DG | Dentate gyrus |
| GCs | Granule cells |
| hAPP | human amyloid precursor protein |
| MCs | Mossy cells |
| MCI | Mild cognitive impairment |
| E/I balance | Excitation/Inhibition balance |
| sEPSPs | Spontaneous excitatory postsynaptic potentials |
| sEPSCs | Spontaneous excitatory postsynaptic currents |
| sIPSCs | Spontaneous inhibitory postsynaptic currents |
| RMP | Resting membrane potential |
| $R_{in}$ | Input resistance |
| τ | Time constant |
| SP | Spikepair |

## Supplementary Information

The online version contains supplementary material available at https://doi.org/10.1186/s13195-025-01747-1.

Supplementary Material 1: Supplementary Fig. 1. Determination of baseline noise. Recordings are shown without and with a filter to improve the signal-to-noise ratio. The red box shows where the determination of noise was made. The arrows point to the sPSCs that were > 3x the standard deviation of the noise measurement.

Supplementary Material 2: Supplementary Fig. 2. Effects of the AMPA receptor antagonist DNQX on sEPSCs recorded at -30 mV. (A) 1. sEPSCs were recorded at -70 mV for AMPA-sEPSCs. 2.Recordings were made at -30 mV for NMDA-sEPSCs. Frequencies are shown during the baseline (Bsln) and after exposure to DNQX (10 μM). Although recordings at -30 mV were previously considered to be appropriate to quantify NMDA-sEPCSs, the sEPSC frequencies were reduced by DNQX, especially in WT mice. (B) (1) sEPSC amplitudes at -70 mV were rare after DNQX but those that were present showed a smaller mean amplitude. Interestingly, the effect of DNQX was only significant for WT mice. (2) sEPSC amplitudes at -30 mV were compared before and after DNQX. There was only a significant reduction in WT mice.

Supplementary Material 3: Supplementary Fig. 3. Comparison of frequency distributions of WT and Tg2576 MCs. For sEPSPs (A), AMPA-sEPSCs (B), and sIPSCs (C) the following measurements were made for each cell (from left to right): skewness, kurtosis, number of values at the peak of the distribution, the percent of total (number of values at the peak relative to the total number of events in the distribution), and the area under the curve (AUC) of the distribution. (A) sEPSPs. Both WT and Tg2576 distributions had a positive skew (a long tail to the right), and positive kurtosis (more extreme values to the right). When comparing genotypes, there were no significant differences in skewness (unpaired t-test; $p = 0.539$) or kurtosis (unpaired t-test; $p = 0.533$), number of values at the peak (Mann-Whitney U test, $p = 0.136$), the percent of that number of values relative to the total number of events in the distribution (unpaired t-test, $p = 0.678$), or the AUC (Welch's test, $p = 0.094$). The data suggest that the shapes of the distributions were similar, differing mainly in the total number of events (WT, 175.6 ± 0.18 events; Tg2576, 587.7 ± 119.8; Mann-Whitney U test, U = 9, $p = 0.003$). (B) AMPA-sEPSCs. There was a trend for skewness to be greater in WT relative to Tg2576 mice (unpaired t-test, t = 2.095, df = 16; $p = 0.053$) and kurtosis was greater in WT mice (Mann-Whitney U test, U = 17; $p = 0.040$). There were a greater number of events at the peak of the distribution in Tg2576 mice (Mann-Whitney U test, U = 4.5; $p < 0.001$), but the percentage of the total number of events was not significantly different (Mann-Whitney U test, $p = 0.915$). The AUC was greater in Tg2576 MCs (Welch's test, t = 3.419, df = 8.000; $p = 0.009$). The results in A and B add support to the findings in Fig. 1 that there are differences between genotypes of sEPSPs and AMPA-sEPSCs, but the characteristics of frequency distributions that differ are not identical. The reason they are not identical may be related to differences in current and voltage clamp discussed in the Results. (C) sIPSCs. Both genotypes showed no significant differences in skewness (unpaired t-test; $p = 0.479$), kurtosis (unpaired t-test; $p = 0.467$), and the number of values at the peak of the distributions (unpaired t-test; $p = 0.577$). However, the percentage of the number of values at the peak relative to the total number of events was lower in WT MCs (unpaired t-test, t = 2.904, df = 16; $p = 0.010$). Also, the AUC was lower in the distributions of Tg2576 MCs (unpaired t-test t = 3.440, df = 16; $p = 0.003$). Therefore, the data suggest a similar shape in the frequency distributions but lower magnitude in Tg2576 MC distributions. These data are consistent with other analyses in Fig. 1.

Supplementary Material 4: Supplementary Fig. 4. MC firing behavior. A. Spike frequency adaptation was quantified in WT and Tg2576 MCs based on a train with 4 APs. (1) The peak-to-peak time was measured for each AP pair (spike-pair, SP) and plotted sequentially. There were no genotype differences. (2) Statistical comparisons of the first and third SP did not show any significant difference in WT and Tg2576 mice. B. Analogous measurements were made for trains with 7 APs (6 SP). (1) For the sequence of 6 SPs, there were no differences between genotypes. (2) Comparisons of the first and sixth SP showed no significant differences. This suggests that MCs from both genotypes did not adapt their firing.

Supplementary Material 5: Supplementary Fig. 5. WT and Tg2576 MCs with similar RMPs differ in their firing behavior. Mean MC firing frequency is plotted for a subset of cells with RMPs between − 65 and − 70 mV which were not significantly different (Tg2576: -68.20 ± 1.13 mV; WT: -68.97 ± 0.76; unpaired t-test, $p = 0.570$). A two-way ANOVA (with genotype and current injected as factors) showed that there were significant differences in genotype ($F(1,8) = 5.834$; $p = 0.042$).

Supplementary Material 6: Supplementary Fig. 6. GC firing behavior. (A) The relationship between AP firing frequency and injected current is plotted for WT and Tg2576 mice. Current steps were injected consecutively, and current was increased in 10 pA increments for each step. The mean firing frequency during each step is plotted. (B) Spike frequency adaptation was quantified in WT and Tg2576 mice based on a train with 4 APs. (1) The peak-to-peak time was measured for each AP pair (spike-pair, SP) and plotted sequentially. There were no genotype differences. (2) Statistical comparisons of the first and third SP did not show any significant difference in WT and Tg2576 mice. C. Analogous measurements were made for trains with 7 APs (6 SPs). (1) For the sequence of 6 SPs, there were no differences between genotypes. (2) Comparisons of the first and sixth SP showed significant differences, suggesting GCs from both genotypes adapted their firing, but there were no significant changes between genotypes.

Supplementary Material 7: Supplementary Fig. 7. Excitation/inhibition balance in WT and Tg2576 GCs A. The ratio of AMPA-EPSCs to IPSCs is shown, based on mean frequency (1) or amplitude (2). E/I ratio based on frequency was increased in Tg2576 mice. B. Charge transfer, which is a reflection of the summed area of PSCs, is shown for AMPA- sEPSCs (1) and sIPSCs (2) and showed no significant difference between genotypes. 3. The E/I ratio for charge transfer based on mean values was reduced in Tg2576 mice, compared with WT mice.

Supplementary Material 8: Supplementary Fig. 8. Rescue of GC synaptic activity in Tg2576 mice by the cannabinoid receptor ligand WIN55212-2. A.1. Comparison of GC AMPA-sEPSC frequency between baseline and after exposure to 10 μM WIN55212-2 in Tg2576 mice. WIN552123-2 blocks excitatory transmission from MCs to GCs [76]. There was a reduction of sEPSC frequency, suggesting that MCs contribute to the increased sEPSCs of Tg2576 GCs. 2. There were no effects of WIN55212-2 Tg2576 mice on sEPSC amplitude, consistent with the presynaptic location of cannabinoid type 1 receptors on MC boutons. B.1–2. WIN55212-2 had no significant

effect on the mean frequency or amplitude of GC sIPSCs in Tg2576 mice. C.1–2. There was a significant decrease in the frequency distributions of Tg2576 GC AMPA-sEPSCs, and a significant increase in the frequency distribution of sIPSCs after WIN55212-2. The lack of effect on means (B1-2) but significant effect on distributions (C1-2) suggests a weaker effect of WIN55212-2 on sIPSCs than sEPSCs. That interpretation is consistent with other studies showing the pharmacology and plasticity of MC→GC synapses differs from MC→GABAergic neurons [71, 72].

Supplementary Material 9: Supplementary Fig. 9. NOR in 1 month-old WT and Tg2576 mice. A. The experimental timeline for the NOR test. Mice were acclimated (1) for three consecutive days. On the 4th day, mice were subjected to a training session (2) and 1 h later mice were tested in the NOR task (3). B. Quantification of novel object exploration (%) during the training and test session for WT and Tg2576 mice. There was no preference for one object over the other during training, but mice increased exploration of the novel object over the familiar one during testing. C. Quantification of the discrimination index during training (1) and testing (2). There were no genotype differences. During the test, the time mice explored the new object was greater than the familiar object, suggesting a preference to explore the new object. D. 1–2. The time that Tg2576 and WT mice spent exploring the new object (1), and the number of approaches mice had to the object (2) did not show significant differences between genotypes. Tg2576 and WT mice had a similar performance in this task, suggesting that DG function is still intact at this age in the Tg2576 mice.

Supplementary Material 10: Supplementary Fig. 10. NOR and NOL in 3.5 months-old WT and Tg2576 mice. A. The experimental timeline of the NOR and NOL tasks. Animals were acclimated for three days before the tasks. B.1. The time spent exploring the novel object (NOR) as a percentage of the total time exploring both objects. 2. The discrimination index for NOR and NOL. Discrimination ratio was defined as the difference in time exploring the novel object vs. familiar object divided by the total time exploring both objects. The results showed that the WT mice performed the task, but Tg2576 mice did not. C.1. The time spent exploring the novel object location (NOL) as a percentage of the total time exploring both objects. 2. The discrimination index for NOL. The results show that the WT mice performed the task, but Tg2576 mice did not.

Supplementary Material 11: Supplementary Table 1. Quantification of baseline noise. Baseline noise was calculated for sEPSPs, sEPSCs recorded at -70 mV, sEPSCs recorded at -30 mV, and sIPSCs recorded at + 10 mV. Data are shown for unfiltered records and after an inverse Chebychev filter with a cut-off frequency of 1000 Hz. The values used for thresholding events (3x the noise) are also shown. There were no significant differences between genotypes (unpaired t-tests). In this table and all others, parametric data were compared using an unpaired Student's t-test (denoted by the number 1) and non-parametric data were compared by a Mann-Whitney test (denoted by the number 2). Also, the statistical significance was set at $p < 0.05$ and data are presented as mean ± SEM.

Supplementary Material 12: Supplementary Table 2. Contributing factors to the two-way ANOVA analysis of MC synaptic distributions. A two-way ANOVA was used to address synaptic activity distributions, with cell ID and genotype as factors. There was a significant effect on both factors for every type of synaptic event.

Supplementary Material 13: Supplementary Table 3. MC intrinsic properties that lacked differences between genotypes. MC intrinsic properties showed no significant differences between genotypes.

Supplementary Material 14: Supplementary Table 4. Intrinsic properties of MCs with −65 to -70 mV RMPs. MCs from WT and Tg2576 mice with RMPs between −65 and −70 mV were compared. There were no significant differences.

Supplementary Material 15: Supplementary Table 5. Lack of sex differences in MC synaptic events. MC sEPSPs were recorded from WT and Tg2576 male and female mice. A two-way ANOVA was used to address sex differences, with sex and genotype as factors. There was no effect of sex. There was a significant effect of genotype for sEPSP frequency (boldface font).

Supplementary Material 16: Supplementary Table 6. Lack of sex differences in MC intrinsic properties. Values of the different intrinsic properties obtained from WT and Tg2576 MCs from male and female mice. Statistical comparisons for evaluating sex differences were performed using a two-way ANOVA with sex and genotype as factors. There were no significant effects of sex but there were effects of genotype (boldface font).

Supplementary Material 17: Supplementary Table 7. Lack of differences of frequency distributions of WT and Tg2576 GCs.

Supplementary Material 18: Supplementary Table 8. Lack of differences between WT and Tg2576 GC intrinsic properties.

Supplementary Material 19: Supplementary Table 9. Intrinsic properties of GCs were similar before and after pharmacological antagonism of synaptic transmission. Values of the different intrinsic properties obtained from WT and Tg2576 GCs during the baseline and after antagonism of synaptic transmission. Statistical comparisons were performed using a two-way ANOVA with treatment and genotype as factors.

Supplementary Material 20: Supplementary Table 10. Differences in WT and Tg2576 GC synaptic events were not influenced by sex. Characteristics of GC sEPSPs, AMPA-sEPSCs, and sIPSCs from WT and Tg2576 mice are shown. A two-way ANOVA with sex and genotype as factors showed significant effects of sex on AMPA-sEPSC amplitude and sIPSC frequency. For sIPSC frequency, there was greater frequency in Tg2576 females compared to Tg2576 males. Thus, the differences in genotypes were not related to sex differences.

Supplementary Material 21: Supplementary Table 11. Sex differences in GC intrinsic properties. GC intrinsic properties from WT and Tg2576 mice are shown. A two-way ANOVA was used to evaluate sex differences with sex and genotype as factors. There was a significant effect of sex on $R_{in}$, rheobase, half-width, and the maximum slope of the AP decay phase. For $R_{in}$, females had lower values. For rheobase, females had higher values. For half-width, females had shorter half-widths than males but only in Tg2576 mice. For the slope of the AP decay, females had a faster repolarization in both genotypes. For threshold, female WT mice had a more hyperpolarized threshold compared to male WT mice, and female Tg2576 mice had a more depolarized threshold than male Tg2576 mice. Thus, there were diverse sex differences, but the comparison of WT and Tg2576 mice was not influenced by sex.

**Acknowledgements**
We thank John LaFrancois for assistance with mice. Declarations of interest: none.

**Author contributions**
DAG: project conceptualization and design, funding acquisition, project administration resources, data acquisition, data analysis, writing and editing the manuscript. HES: conceptualization and design, funding acquisition, administrative resources, editing, supervision. MK, CC and JB participated in the animal model generation and provided advice on data collection. The authors read and approved the final manuscript.

**Funding**
This research was supported by the Alzheimer's Association, AARFD-22-926807 for DAG, and NIH R01 AG-055328 to H.E.S. and the New York State Office of Mental Health.

**Data availability**
The datasets supporting the conclusions of this article are available in the Open Science Framework repository, https://osf.io/fj5rk/?view_only=d31fb7f34e32439490e4f2ddb58f860f. Other datasets supporting the conclusions of this study are included in this published article and its supplementary information files (supplementary tables).

## Declarations

**Ethics approval and consent to participate**
Not applicable.

**Consent for publication**
Not applicable.

**Competing interests**
The authors declare no competing interests.

Received: 7 March 2024 / Accepted: 22 April 2025
Published online: 15 May 2025

**References**

1. Wang JZ, Xia YY, Grundke-Iqbal I, Iqbal K. Abnormal hyperphosphorylation of Tau: sites, regulation, and molecular mechanism of neurofibrillary degeneration. J Alzheimers Dis. 2013;33(Suppl 1):S123–39.
2. Walsh DM, Selkoe DJ. Aβ oligomers - a decade of discovery. J Neurochem. 2007;101:1172–84.
3. Lue LF, Kuo YM, Roher AE, Brachova L, Shen Y, Sue L, et al. Soluble amyloid B peptide concentration as a predictor of synaptic change in Alzheimer's disease. Am J Pathol. 1999;155:853–62.
4. Braak H, Braak E. Neuropathological stageing of Alzheimer-related changes. Acta Neuropathol. 1991;82:239–59.
5. Palop JJ, Mucke L. Epilepsy and cognitive impairments in Alzheimer disease. Arch Neurol. 2009;66:435–40.
6. Palop JJ, Mucke L. Synaptic depression and aberrant excitatory network activity in Alzheimer's disease: two faces of the same coin? Neuromol Med. 2010;12:48–55.
7. Vossel KA, Tartaglia MC, Nygaard HB, Zeman AZ, Miller BL. Epileptic activity in Alzheimer's disease: causes and clinical relevance. Lancet Neurol. 2017;16:311–22.
8. Noebels J. A perfect storm: converging paths of epilepsy and Alzheimer's dementia intersect in the hippocampal formation. Epilepsia. 2011;52(Suppl 1):39–46.
9. Friedman D, Honig LS, Scarmeas N. Seizures and epilepsy in Alzheimer's disease. CNS Neurosci Ther. 2012;18:285–94.
10. Vossel KA, Beagle AJ, Rabinovici GD, Shu H, Lee SE, Naasan G, et al. Seizures and epileptiform activity in the early stages of Alzheimer disease. JAMA Neurol. 2013;70:1158–66.
11. Styr B, Slutsky I. Imbalance between firing homeostasis and synaptic plasticity drives early-phase Alzheimer's disease. Nat Neurosci. 2018;21:463–73.
12. Celone KA, Calhoun VD, Dickerson BC, Atri A, Chua EF, Miller SL, et al. Alterations in memory networks in mild cognitive impairment and Alzheimer's disease: an independent component analysis. J Neurosci. 2006;26:10222–31.
13. Dickerson BC, Salat DH, Greve DN, Chua EF, Rand-Giovannetti E, Rentz DM, et al. Increased hippocampal activation in mild cognitive impairment compared to normal aging and AD. Neurology. 2005;65:404–11.
14. Scarmeas N, Honig LS, Choi H, Cantero J, Brandt J, Blacker D, et al. Seizures in Alzheimer disease: who, when, and how common? Arch Neurol. 2009;66:992–7.
15. Leonard AS, McNamara JO. Does epileptiform activity contribute to cognitive impairment in Alzheimer's disease? Neuron. 2007;55:677–8.
16. Palop JJ, Chin J, Roberson ED, Wang J, Thwin MT, Bien-Ly N, et al. Aberrant excitatory neuronal activity and compensatory remodeling of inhibitory hippocampal circuits in mouse models of Alzheimer's disease. Neuron. 2007;55:697–711.
17. Scharfman HE. Alzheimer's disease and epilepsy: insight from animal models. Future Neurol. 2012;7:177–92.
18. Chin J, Scharfman HE. Shared cognitive and behavioral impairments in epilepsy and Alzheimer's disease and potential underlying mechanisms. Epilepsy Behav. 2013;26:343–51.
19. Siskova Z, Justus D, Kaneko H, Friedrichs D, Henneberg N, Beutel T, et al. Dendritic structural degeneration is functionally linked to cellular hyperexcitability in a mouse model of Alzheimer's disease. Neuron. 2014;84:1023–33.
20. Minkeviciene R, Rheims S, Dobszay MB, Zilberter M, Hartikainen J, Fulop L, et al. Amyloid β-induced neuronal hyperexcitability triggers progressive epilepsy. J Neurosci. 2009;29:3453–62.
21. Gail Canter R, Huang WC, Choi H, Wang J, Ashley Watson L, Yao CG, et al. 3D mapping reveals network-specific amyloid progression and subcortical susceptibility in mice. Commun Biol. 2019;2:360.
22. Gotz J, Bodea LG, Goedert M. Rodent models for Alzheimer disease. Nat Rev Neurosci. 2018;19:583–98.
23. Kam K, Duffy AM, Moretto J, LaFrancois JJ, Scharfman HE. Interictal spikes during sleep are an early defect in the Tg2576 mouse model of β-amyloid neuropathology. Sci Rep. 2016;6:20119.
24. Bezzina C, Verret L, Juan C, Remaud J, Halley H, Rampon C, et al. Early onset of hypersynchronous network activity and expression of a marker of chronic seizures in the Tg2576 mouse model of Alzheimer's disease. PLoS ONE. 2015;10:e0119910.
25. Lisgaras CP, Scharfman HE. High-frequency oscillations (250–500 Hz) in animal models of Alzheimer's disease and two animal models of epilepsy. Epilepsia. 2023;64:231–46.
26. Ziyatdinova S, Ronnback A, Gurevicius K, Miszczuk D, Graff C, Winblad B, et al. Increased epileptiform EEG activity and decreased seizure threshold in arctic APP transgenic mouse model of Alzheimer's disease. Curr Alzheimer Res. 2016;13:817–30.
27. Alcantara-Gonzalez D, Villasana-Salazar B, Pena-Ortega F. Single amyloid-β injection exacerbates 4-aminopyridine-induced seizures and changes synaptic coupling in the hippocampus. Hippocampus. 2019;29:1150–64.
28. Beckman M, Knox K, Koneval Z, Smith C, Jayadev S, Barker-Haliski M. Loss of presenilin 2 age-dependently alters susceptibility to acute seizures and kindling acquisition. Neurobiol Dis. 2020;136:104719.
29. Gheyara AL, Ponnusamy R, Djukic B, Craft RJ, Ho K, Guo W, et al. Tau reduction prevents disease in a mouse model of Dravet syndrome. Ann Neurol. 2014;76:443–56.
30. Bakker A, Krauss GL, Albert MS, Speck CL, Jones LR, Stark CE, et al. Reduction of hippocampal hyperactivity improves cognition in amnestic mild cognitive impairment. Neuron. 2012;74:467–74.
31. Verret L, Mann EO, Hang GB, Barth AM, Cobos I, Ho K, et al. Inhibitory interneuron deficit links altered network activity and cognitive dysfunction in alzheimer model. Cell. 2012;149:708–21.
32. Vossel KA, Zhang K, Brodbeck J, Daub AC, Sharma P, Finkbeiner S, et al. Tau reduction prevents Aβ-induced defects in axonal transport. Science. 2010;330:198.
33. Sanchez PE, Zhu L, Verret L, Vossel KA, Orr AG, Cirrito JR, et al. Levetiracetam suppresses neuronal network dysfunction and reverses synaptic and cognitive deficits in an Alzheimer's disease model. Proc Natl Acad Sci U S A. 2012;109:E2895–903.
34. Roberson ED, Scearce-Levie K, Palop JJ, Yan F, Cheng IH, Wu T, et al. Reducing endogenous Tau ameliorates amyloid β-induced deficits in an Alzheimer's disease mouse model. Science. 2007;316:750–4.
35. Bonilha L, Kobayashi E, Rorden C, Cendes F, Li LM. Medial temporal lobe atrophy in patients with refractory temporal lobe epilepsy. J Neurol Neurosurg Psychiatry. 2003;74:1627–30.
36. Cendes F. Progressive hippocampal and extrahippocampal atrophy in drug resistant epilepsy. Curr Opin Neurol. 2005;18:173–7.
37. Palop JJ, Jones B, Kekonius L, Chin J, Yu GQ, Raber J, et al. Neuronal depletion of calcium-dependent proteins in the dentate gyrus is tightly linked to Alzheimer's disease-related cognitive deficits. Proc Natl Acad Sci U S A. 2003;100:9572–7.
38. Dengler CG, Coulter DA. Normal and epilepsy-associated pathologic function of the dentate gyrus. Prog Brain Res. 2016;226:155–78.
39. Neunuebel JP, Knierim JJ. Spatial firing correlates of physiologically distinct cell types of the rat dentate gyrus. J Neurosci. 2012;32:3848–58.
40. Fricke RA, Prince DA. Electrophysiology of dentate gyrus granule cells. J Neurophysiol. 1984;51:195–209.
41. Staley KJ, Otis TS, Mody I. Membrane properties of dentate gyrus granule cells: comparison of sharp microelectrode and whole-cell recordings. J Neurophysiol. 1992;67:1346–58.
42. Houser CR. Interneurons of the dentate gyrus: an overview of cell types, terminal fields and neurochemical identity. Prog Brain Res. 2007;163:217–32.
43. Coulter DA, Carlson GC. Functional regulation of the dentate gyrus by GABA-mediated inhibition. Prog Brain Res. 2007;163:235–43.
44. Ewell LA, Jones MV. Frequency-tuned distribution of inhibition in the dentate gyrus. J Neurosci. 2010;30:12597–607.
45. Heinemann U, Beck H, Dreier JP, Ficker E, Stabel J, Zhang CL. The dentate gyrus as a regulated gate for the propagation of epileptiform activity. Epilepsy Res Suppl. 1992;7:273–80.
46. Krook-Magnuson E, Armstrong C, Bui A, Lew S, Oijala M, Soltesz I. In vivo evaluation of the dentate gate theory in epilepsy. J Physiol. 2015;593:2379–88.
47. Leutgeb JK, Leutgeb S, Moser MB, Moser EI. Pattern separation in the dentate gyrus and CA3 of the hippocampus. Science. 2007;315:961–6.
48. Amaral DG, Scharfman HE, Lavenex P. The dentate gyrus: fundamental neuroanatomical organization (dentate gyrus for dummies). Prog Brain Res. 2007;163:3–22.
49. Scharfman HE. The dentate gyrus and temporal lobe epilepsy: an exciting era. Epilepsy Curr. 2019;19:249–55.

50. Parizkova M, Lerch O, Andel R, Kalinova J, Markova H, Vyhnalek M, et al. Spatial pattern separation in early Alzheimer's disease. J Alzheimers Dis. 2020;76:121–38.
51. Hsiao K, Chapman P, Nilsen S, Eckman C, Harigaya Y, Younkin S, et al. Correlative memory deficits, Aβ elevation, and amyloid plaques in transgenic mice. Science. 1996;274:99–102.
52. Citron M, Oltersdorf T, Haass C, McConlogue L, Hung AY, Seubert P, et al. Mutation of the β-amyloid precursor protein in familial Alzheimer's disease increases β-protein production. Nature. 1992;360:672–4.
53. Kawarabayashi T, Younkin LH, Saido TC, Shoji M, Ashe KH, Younkin SG. Age-dependent changes in brain, CSF, and plasma amyloid (β) protein in the Tg2576 transgenic mouse model of Alzheimer's disease. J Neurosci. 2001;21:372–81.
54. Jacobsen JS, Wu CC, Redwine JM, Comery TA, Arias R, Bowlby M, et al. Early-onset behavioral and synaptic deficits in a mouse model of Alzheimer's disease. Proc Natl Acad Sci U S A. 2006;103:5161–6.
55. Alcantara-Gonzalez D, Chartampila E, Criscuolo C, Scharfman HE. Early changes in synaptic and intrinsic properties of dentate gyrus granule cells in a mouse model of Alzheimer's disease neuropathology and atypical effects of the cholinergic antagonist Atropine. Neurobiol Dis. 2021;152:105274.
56. Buckmaster PS, Wenzel HJ, Kunkel DD, Schwartzkroin PA. Axon arbors and synaptic connections of hippocampal mossy cells in the rat in vivo. J Comp Neurol. 1996;366:271–92.
57. Scharfman HE, Schwartzkroin PA. Electrophysiology of morphologically identified mossy cells of the dentate hilus recorded in guinea pig hippocampal slices. J Neurosci. 1988;8:3812–21.
58. Livsey CT, Vicini S. Slower spontaneous excitatory postsynaptic currents in spiny versus aspiny hilar neurons. Neuron. 1992;8:745–55.
59. Scharfman HE. Characteristics of spontaneous and evoked EPSPs recorded from dentate spiny hilar cells in rat hippocampal slices. J Neurophysiol. 1993;70:742–57.
60. Scharfman HE, Myers CE. Hilar mossy cells of the dentate gyrus: a historical perspective. Front Neural Circuits. 2012;6:106.
61. Ribak CE, Seress L, Amaral DG. The development, ultrastructure and synaptic connections of the mossy cells of the dentate gyrus. J Neurocytol. 1985;14:835–57.
62. Botterill JJ, Gerencer KJ, Vinod KY, Alcantara-Gonzalez D, Scharfman HE. Dorsal and ventral mossy cells differ in their axonal projections throughout the dentate gyrus of the mouse hippocampus. Hippocampus. 2021;31:522–39.
63. Scharfman HE. Electrophysiological evidence that dentate hilar mossy cells are excitatory and innervate both granule cells and interneurons. J Neurophysiol. 1995;74:179–94.
64. Larimer P, Strowbridge BW. Nonrandom local circuits in the dentate gyrus. J Neurosci. 2008;28:12212–23.
65. Bernstein HL, Lu Y-L, Botterill JJ, Duffy ÁM, LaFrancois JJ, Scharfman HE. Excitatory effects of dentate gyrus mossy cells and their ability to influence granule cell firing: an optogenetic study in adult mouse hippocampal slices. BioRxiv. 2020:2020.06.06.137844.
66. Sloviter RS. Permanently altered hippocampal structure, excitability, and inhibition after experimental status epilepticus in the rat: the dormant basket cell hypothesis and its possible relevance to temporal lobe epilepsy. Hippocampus. 1991;1:41–66.
67. Sloviter RS. The functional organization of the hippocampal dentate gyrus and its relevance to the pathogenesis of temporal lobe epilepsy. Ann Neurol. 1994;35:640–54.
68. Jinde S, Zsiros V, Jiang Z, Nakao K, Pickel J, Kohno K, et al. Hilar mossy cell degeneration causes transient dentate granule cell hyperexcitability and impaired pattern separation. Neuron. 2012;76:1189–200.
69. Bui AD, Nguyen TM, Limouse C, Kim HK, Szabo GG, Felong S, et al. Dentate gyrus mossy cells control spontaneous convulsive seizures and spatial memory. Science. 2018;359:787–90.
70. Botterill JJ, Lu YL, LaFrancois JJ, Bernstein HL, Alcantara-Gonzalez D, Jain S, et al. An excitatory and epileptogenic effect of dentate gyrus mossy cells in a mouse model of epilepsy. Cell Rep. 2019;29:2875–89. e6.
71. Nasrallah K, Berthoux C, Hashimotodani Y, Chavez AE, Gulfo MC, Lujan R, et al. Retrograde adenosine/A(2A) receptor signaling facilitates excitatory synaptic transmission and seizures. Cell Rep. 2024;43:114382.
72. Nasrallah K, Frechou MA, Yoon YJ, Persaud S, Goncalves JT, Castillo PE. Seizure-induced strengthening of a recurrent excitatory circuit in the dentate gyrus is proconvulsant. Proc Natl Acad Sci U S A. 2022;119:e2201151119.
73. Scharfman HE. The enigmatic mossy cell of the dentate gyrus. Nat Rev Neurosci. 2016;17:562–75.
74. Hong SL, Rebec GV. A new perspective on behavioral inconsistency and neural noise in aging: compensatory speeding of neural communication. Front Aging Neurosci. 2012;4:27.
75. Serletis D, Zalay OC, Valiante TA, Bardakjian BL, Carlen PL. Complexity in neuronal noise depends on network interconnectivity. Ann Biomed Eng. 2011;39:1768–78.
76. Chiu CQ, Castillo PE. Input-specific plasticity at excitatory synapses mediated by endocannabinoids in the dentate gyrus. Neuropharmacology. 2008;54:68–78.
77. Watt AJ, van Rossum MC, MacLeod KM, Nelson SB, Turrigiano GG. Activity coregulates quantal AMPA and NMDA currents at neocortical synapses. Neuron. 2000;26:659–70.
78. Burzomato V, Frugier G, Perez-Otano I, Kittler JT, Attwell D. The receptor subunits generating NMDA receptor mediated currents in oligodendrocytes. J Physiol. 2010;588:3403–14.
79. Blasco-Ibanez JM, Freund TF. Distribution, ultrastructure, and connectivity of calretinin-immunoreactive mossy cells of the mouse dentate gyrus. Hippocampus. 1997;7:307–20.
80. Fujise N, Liu Y, Hori N, Kosaka T. Distribution of calretinin immunoreactivity in the mouse dentate gyrus: II. Mossy cells, with special reference to their dorsoventral difference in calretinin immunoreactivity. Neuroscience. 1998;82:181–200.
81. Takeda A, Tamano H, Ogawa T, Takada S, Nakamura M, Fujii H, et al. Intracellular Zn(2+) signaling in the dentate gyrus is required for object recognition memory. Hippocampus. 2014;24:1404–12.
82. Bernstein HL, Lu YL, Botterill JJ, Scharfman HE. Novelty and novel objects increase c-Fos immunoreactivity in mossy cells in the mouse dentate gyrus. Neural Plast. 2019;2019:1815371.
83. Duffy AM, Schaner MJ, Chin J, Scharfman HE. Expression of c-fos in hilar mossy cells of the dentate gyrus in vivo. Hippocampus. 2013;23:649–55.
84. Guzowski JF, Timlin JA, Roysam B, McNaughton BL, Worley PF, Barnes CA. Mapping behaviorally relevant neural circuits with immediate-early gene expression. Curr Opin Neurobiol. 2005;15:599–606.
85. Chung L. A brief introduction to the transduction of neural activity into Fos signal. Dev Reprod. 2015;19:61–7.
86. Duffy AM, Morales-Corraliza J, Bermudez-Hernandez KM, Schaner MJ, Magagna-Poveda A, Mathews PM, et al. Entorhinal cortical defects in Tg2576 mice are present as early as 2–4 months of age. Neurobiol Aging. 2015;36:134–48.
87. Chen C. β-Amyloid increases dendritic Ca2 + influx by inhibiting the A-type K + current in hippocampal CA1 pyramidal neurons. Biochem Biophys Res Commun. 2005;338:1913–9.
88. Chen QS, Wei WZ, Shimahara T, Xie CW. Alzheimer amyloid β-peptide inhibits the late phase of long-term potentiation through calcineurin-dependent mechanisms in the hippocampal dentate gyrus. Neurobiol Learn Mem. 2002;77:354–71.
89. Ciccone R, Franco C, Piccialli I, Boscia F, Casamassa A, de Rosa V, et al. Amyloid β-induced upregulation of Nav1.6 underlies neuronal hyperactivity in Tg2576 Alzheimer's disease mouse model. Sci Rep. 2019;9:13592.
90. Eslamizade MJ, Saffarzadeh F, Mousavi SM, Meftahi GH, Hosseinmardi N, Mehdizadeh M, et al. Alterations in CA1 pyramidal neuronal intrinsic excitability mediated by ih channel currents in a rat model of amyloid β pathology. Neuroscience. 2015;305:279–92.
91. Hou JF, Cui J, Yu LC, Zhang Y. Intracellular amyloid induces impairments on electrophysiological properties of cultured human neurons. Neurosci Lett. 2009;462:294–9.
92. Pena F, Ordaz B, Balleza-Tapia H, Bernal-Pedraza R, Marquez-Ramos A, Carmona-Aparicio L, et al. β-amyloid protein (25–35) disrupts hippocampal network activity: role of Fyn-kinase. Hippocampus. 2010;20:78–96.
93. Rovira C, Arbez N, Mariani J. Aβ(25–35) and Aβ(1–40) act on different calcium channels in CA1 hippocampal neurons. Biochem Biophys Res Commun. 2002;296:1317–21.
94. Tamagnini F, Scullion S, Brown JT, Randall AD. Intrinsic excitability changes induced by acute treatment of hippocampal CA1 pyramidal neurons with exogenous amyloid β peptide. Hippocampus. 2015;25:786–97.
95. Wu J, Anwyl R, Rowan MJ. β-Amyloid selectively augments NMDA receptor-mediated synaptic transmission in rat hippocampus. NeuroReport. 1995;6:2409–13.
96. Rahimi O, Claiborne BJ. Morphological development and maturation of granule neuron dendrites in the rat dentate gyrus. Prog Brain Res. 2007;163:167–81.

97. Botterill JJ, Vinod KY, Gerencer KJ, Teixeira CM, LaFrancois JJ, Scharfman HE. Bidirectional regulation of cognitive and anxiety-like behaviors by dentate gyrus mossy cells in male and female mice. J Neurosci. 2021;41:2475–95.
98. Lothman EW, Stringer JL, Bertram EH. The dentate gyrus as a control point for seizures in the hippocampus and beyond. Epilepsy Res Suppl. 1992;7:301–13.
99. Williams PA, Larimer P, Gao Y, Strowbridge BW. Semilunar granule cells: glutamatergic neurons in the rat dentate gyrus with axon collaterals in the inner molecular layer. J Neurosci. 2007;27:13756–61.
100. Toni N, Laplagne DA, Zhao C, Lombardi G, Ribak CE, Gage FH, et al. Neurons born in the adult dentate gyrus form functional synapses with target cells. Nat Neurosci. 2008;11:901–7.
101. Scharfman HE. Evidence from simultaneous intracellular recordings in rat hippocampal slices that area CA3 pyramidal cells innervate dentate hilar mossy cells. J Neurophysiol. 1994;72:2167–80.
102. Scharfman HE. Dentate hilar cells with dendrites in the molecular layer have lower thresholds for synaptic activation by perforant path than granule cells. J Neurosci. 1991;11:1660–73.
103. Azevedo EP, Pomeranz L, Cheng J, Schneeberger M, Vaughan R, Stern SA, et al. A role of Drd2 hippocampal neurons in context-dependent food intake. Neuron. 2019;102:873–86. e5.
104. Scharfman HE, Chao MV. The entorhinal cortex and neurotrophin signaling in Alzheimer's disease and other disorders. Cogn Neurosci. 2013;4:123–35.
105. Sun Y, Grieco SF, Holmes TC, Xu X. Local and long-range circuit connections to hilar mossy cells in the dentate gyrus. eNeuro. 2017;4.
106. Hazra A, Gu F, Aulakh A, Berridge C, Eriksen JL, Ziburkus J. Inhibitory neuron and hippocampal circuit dysfunction in an aged mouse model of Alzheimer's disease. PLoS ONE. 2013;8:e64318.
107. Martinez-Losa M, Tracy TE, Ma K, Verret L, Clemente-Perez A, Khan AS, et al. Nav1.1-overexpressing interneuron transplants restore brain rhythms and cognition in a mouse model of Alzheimer's disease. Neuron. 2018;98:75–89. e5.
108. Perez C, Ziburkus J, Ullah G. Analyzing and modeling the dysfunction of inhibitory neurons in Alzheimer's disease. PLoS ONE. 2016;11:e0168800.
109. Witton J, Staniaszek LE, Bartsch U, Randall AD, Jones MW, Brown JT. Disrupted hippocampal sharp-wave ripple-associated spike dynamics in a transgenic mouse model of dementia. J Physiol. 2016;594:4615–30.
110. Deller T, Katona I, Cozzari C, Frotscher M, Freund TF. Cholinergic innervation of mossy cells in the rat fascia dentata. Hippocampus. 1999;9:314–20.
111. Nyakas C, Luiten PG, Spencer DG, Traber J. Detailed projection patterns of septal and diagonal band efferents to the hippocampus in the rat with emphasis on innervation of CA1 and dentate gyrus. Brain Res Bull. 1987;18:533–45.
112. Clarke DJ. Cholinergic innervation of the rat dentate gyrus: an immunocytochemical and electron microscopical study. Brain Res. 1985;360:349–54.
113. Leranth C, Frotscher M. Cholinergic innervation of hippocampal GAD- and somatostatin-immunoreactive commissural neurons. J Comp Neurol. 1987;261:33–47.
114. Takacs VT, Cserep C, Schlingloff D, Posfai B, Szonyi A, Sos KE, et al. Co-transmission of acetylcholine and GABA regulates hippocampal States. Nat Commun. 2018;9:2848.
115. Dougherty KD, Milner TA. Cholinergic septal afferent terminals preferentially contact neuropeptide Y-containing interneurons compared to parvalbumin-containing interneurons in the rat dentate gyrus. J Neurosci. 1999;19:10140–52.
116. Frazier CJ, Strowbridge BW, Papke RL. Nicotinic receptors on local circuit neurons in dentate gyrus: a potential role in regulation of granule cell excitability. J Neurophysiol. 2003;89:3018–28.
117. Chiang PH, Yeh WC, Lee CT, Weng JY, Huang YY, Lien CC. M(1)-like muscarinic acetylcholine receptors regulate fast-spiking interneuron excitability in rat dentate gyrus. Neuroscience. 2010;169:39–51.
118. Raza SA, Albrecht A, Caliskan G, Muller B, Demiray YE, Ludewig S, et al. HIPP neurons in the dentate gyrus mediate the cholinergic modulation of background context memory salience. Nat Commun. 2017;8:189.
119. Dannenberg H, Young K, Hasselmo M. Modulation of hippocampal circuits by muscarinic and nicotinic receptors. Front Neural Circuits. 2017;11:102.
120. Yi F, Ball J, Stoll KE, Satpute VC, Mitchell SM, Pauli JL, et al. Direct excitation of parvalbumin-positive interneurons by M1 muscarinic acetylcholine receptors: roles in cellular excitability, inhibitory transmission and cognition. J Physiol. 2014;592:3463–94.
121. Pabst M, Braganza O, Dannenberg H, Hu W, Pothmann L, Rosen J, et al. Astrocyte intermediaries of septal cholinergic modulation in the hippocampus. Neuron. 2016;90:853–65.
122. Gulisano W, Melone M, Ripoli C, Tropea MR, Li Puma DD, Giunta S, et al. Neuromodulatory action of picomolar extracellular Aβ42 oligomers on presynaptic and postsynaptic mechanisms underlying synaptic function and memory. J Neurosci. 2019;39:5986–6000.
123. Parameshwaran K, Sims C, Kanju P, Vaithianathan T, Shonesy BC, Dhanasekaran M, et al. Amyloid β-peptide Aβ(1–42) but not Aβ(1–40) attenuates synaptic AMPA receptor function. Synapse. 2007;61:367–74.
124. Yao W, Zou HJ, Sun D, Ren SQ. Aβ induces acute depression of excitatory glutamatergic synaptic transmission through distinct phosphatase-dependent mechanisms in rat CA1 pyramidal neurons. Brain Res. 2013;1515:88–97.
125. Ripoli C, Cocco S, Li Puma DD, Piacentini R, Mastrodonato A, Scala F, et al. Intracellular accumulation of amyloid-β(Aβ) protein plays a major role in Aβ-induced alterations of glutamatergic synaptic transmission and plasticity. J Neurosci. 2014;34:12893–903.
126. Xu W, Fitzgerald S, Nixon RA, Levy E, Wilson DA. Early hyperactivity in lateral entorhinal cortex is associated with elevated levels of Aβ PP metabolites in the Tg2576 mouse model of Alzheimer's disease. Exp Neurol. 2015;264:82–91.
127. Nixon RA. Amyloid precursor protein and endosomal-lysosomal dysfunction in Alzheimer's disease: inseparable partners in a multifactorial disease. FASEB J. 2017;31:2729–43.
128. Johnson ECB, Ho K, Yu GQ, Das M, Sanchez PE, Djukic B, et al. Behavioral and neural network abnormalities in human APP transgenic mice resemble those of APP knock-in mice and are modulated by familial Alzheimer's disease mutations but not by inhibition of BACE1. Mol Neurodegener. 2020;15:53.
129. Li S, Wang X, Ma QH, Yang WL, Zhang XG, Dawe GS, et al. Amyloid precursor protein modulates Nav1.6 sodium channel currents through a Go-coupled JNK pathway. Sci Rep. 2016;6:39320.
130. Houser CR, Peng Z, Wei X, Huang CS, Mody I. Mossy cells in the dorsal and ventral dentate gyrus differ in their patterns of axonal projections. J Neurosci. 2021;41:991–1004.
131. Francis BM, Kim J, Barakat ME, Fraenkl S, Yucel YH, Peng S, et al. Object recognition memory and BDNF expression are reduced in young TgCRND8 mice. Neurobiol Aging. 2012;33:555–63.
132. You JC, Muralidharan K, Park JW, Petrof I, Pyfer MS, Corbett BF, et al. Epigenetic suppression of hippocampal calbindin-D28k by DeltaFosB drives seizure-related cognitive deficits. Nat Med. 2017;23:1377–83.
133. Beam CR, Kaneshiro C, Jang JY, Reynolds CA, Pedersen NL, Gatz M. Differences between women and men in incidence rates of dementia and Alzheimer's disease. J Alzheimers Dis. 2018;64:1077–83.
134. Clinton LK, Billings LM, Green KN, Caccamo A, Ngo J, Oddo S, et al. Age-dependent sexual dimorphism in cognition and stress response in the 3xTg-AD mice. Neurobiol Dis. 2007;28:76–82.
135. Yang JT, Wang ZJ, Cai HY, Yuan L, Hu MM, Wu MN, et al. Sex differences in neuropathology and cognitive behavior in APP/PS1/tau triple-transgenic mouse model of Alzheimer's disease. Neurosci Bull. 2018;34:736–46.
136. Roy U, Stute L, Hofling C, Hartlage-Rubsamen M, Matysik J, Robetaner S, et al. Sex- and age-specific modulation of brain GABA levels in a mouse model of Alzheimer's disease. Neurobiol Aging. 2018;62:168–79.
137. Jiao SS, Bu XL, Liu YH, Zhu C, Wang QH, Shen LL, et al. Sex dimorphism profile of Alzheimer's disease-type pathologies in an APP/PS1 mouse model. Neurotox Res. 2016;29:256–66.
138. Bangasser DA, Dong H, Carroll J, Plona Z, Ding H, Rodriguez L, et al. Corticotropin-releasing factor overexpression gives rise to sex differences in Alzheimer's disease-related signaling. Mol Psychiatry. 2017;22:1126–33.


## Publisher's note

Springer Nature remains neutral with regard to jurisdictional claims in published maps and institutional affiliations.